This paper appears in Control Engineering Practice, 2020.


# Assist-as-needed Policy for Movement Therapy Using Telerobotics-mediated Therapist Supervision

Mojtaba Sharifi [a,b,c], Saeed Behzadipour [c,*], Hassan Salarieh [c] and Mahdi Tavakoli [a]

[a] *Department of Electrical and Computer Engineering, University of Alberta, Edmonton, Alberta, T6G 1H9, Canada*
[b] *Department of Medicine, Division of Physical Medicine and Rehabilitation, University of Alberta, Edmonton, Alberta, T6G 2E1, Canada*
[c] *Department of Mechanical Engineering, Sharif University of Technology, Tehran, 11155-9567, Iran*

## Abstract

In this paper, a new impedance-based teleoperation strategy is proposed for assist-as-needed tele-rehabilitation via a multi-DOF telerobotic system having patient-master and therapist-slave interactions. Unlike a regular teleoperation system and as the main contribution of this work to minimize the therapist's movements, the therapist's hand only follows the patient's deviation from the target trajectory and not the total patient's motion. The admissible deviation of the patient's limb from a reference target trajectory is governed by an impedance model responding to both patient's and therapist's interaction forces. As the other benefit of this framework, two sources of assistance to the patient are delivered through the master robot: 1) the adjustable impedance model, and 2) the force applied by the therapist to the slave robot. The assistive impedance model is beneficial to reduce magnitudes of the required force from the therapist and decrease his/her intervention. This results in delaying and declining the therapist's muscle fatigue in time-consuming movement therapies. Bilateral nonlinear control laws with two types of adaptation laws are designed for the nonlinear teleoperation system. The Lyapunov stability proof of the teleoperation system and the stability of the impedance model enhance the patient's and therapist's safety even in the presence of modeling uncertainties of the multi-DOF telerobotic system. The performance of the proposed bilateral impedance-based strategy is experimentally investigated using different impedance parameters adjusted based on the patient's characteristics (e.g., involuntary tremor) and disabilities (e.g., insufficient actuation force). The experiments are performed by a healthy person (as the therapist), a mechanical test bed and a volunteer (simulating the patients' characteristics). A new force-position mapping from Cartesian to Normal-Tangential (N-T) coordinates is utilized between the master and slave workspaces and compared with typical Cartesian to Cartesian projection.

**Keywords:** Assist-as-needed tele-rehabilitation, patient-therapist collaboration, bilateral telerobotic system, impedance control, nonlinear adaptive control, Lyapunov stability.

## 1. Introduction

Stroke, multiple sclerosis, and Parkinson's disease are age-related disorders that cause various forms of disability and require rehabilitation programs for the patient. Stroke is the second leading cause of death worldwide [1] and one of the main causes of serious long-term disabilities among adults. There are 6.6 million stroke survivors only in the United States and the estimated annual cost for treatment and care of the affected patients is over $33 billion [2]. Rehabilitation of the stroke patients using movement therapy is achieved due to the neuroplasticity of the brain [3]. Neuroplasticity refers to the ability of the brain and other parts of the central nervous system

* Corresponding author.

E-mail addresses: sharifi3@ualberta.ca, m.sharifi@shirazu.ac.ir (M. Sharifi), behzadipour@sharif.edu (S. Behzadipour), salarieh@sharif.edu (H. Salarieh), mahdi.tavakoli@ualberta.ca (M. Tavakoli).

to reorganize itself [4]. Neuroplastic development in the structure and function of brain-related areas can be induced using rehabilitation methods. The therapeutic method (e.g., movement therapy) that induces neuroplastic changes can provide rapid motor and functional recovery [3]. Since the required intensive rehabilitation of the patients is costly, robotic systems have been developed to provide consistent and reproducible rehabilitation services to patients with less fatigue for therapists [5-7]. Robot manipulators can perform intensive, reproducible and task-specific movement therapies [3, 8] in addition to realizing different physical interactions in active, assistive, or resistive exercises [9]. Most robotic rehabilitation systems developed in the past two decades involve only one robot manipulator interacting with the patient's limb [8, 10-13]. A second robot, however, may provide an online role for the therapist to monitor and/or guide the exercise. Therefore, a bilateral telerobotic system can provide a cooperative tele-rehabilitation environment that allows the therapist and the patient to interact with each other during the therapy process.

In recent years, some robotic systems [14-23] have been used for remote rehabilitation applications. Unilateral [17, 18] and bilateral [19, 20, 24] control strategies have been suggested for tele-rehabilitation using a shared virtual environment (SVE). Most of these methods have employed the position of both robots in the SVE [17-20] and benefited from the force measurements [21, 24] to reflect the haptic force feedback in the teleoperation system. Various control methods have been presented for single-DOF (linear) teleoperation systems [25-28]. However, in order to perform complex and dexterous therapy exercises, multi-DOF (nonlinear) teleoperation systems are required. Bilateral adaptive control methods have been designed to synchronize the positions of nonlinear master and slave robots [29-31] and reflect their interaction forces [32, 33].

The control objective of robotic systems can be modified from pure position or force control to impedance and/or admittance control in order to be augmented by mechanical flexibilities to conduct more physically challenging tasks. Accordingly, impedance/admittance control theory [34-36] has been employed to facilitate the performance of interactive rehabilitation tasks during the interaction of a patient with a robot [11, 37]. The impedance control method has also been used for one-DOF linear bilateral telerobotic systems [38-41]. Also, an impedance model with a damping element for both master and slave robots was suggested in [42].

In the present work, a new nonlinear bilateral adaptive impedance-based control strategy is developed for assistive tele-rehabilitation scenarios involving a nonlinear multi-DOF telerobotic system. This control strategy has the following characteristics and novelties in comparison with the prior art:

1) A new scheme for cooperation between the patient and therapist in tracking a moving target (for movement therapy) is defined. In this method, the patient's flexibility (admissible deviation from the target position) is controlled in relation to the patient's and therapist's forces applied to the master and slave robots, respectively. This feature is achieved by enforcing a desired impedance model for the teleoperation system as a mediator that relates the desired positions to the interaction forces, unlike the previous nonlinear bilateral controllers [32, 33, 43, 44] that involve pure position and/or force tracking control strategies. Also, unlike the previous studies [45-48] on robotic tele-rehabilitation systems in which two or more impedance models were taken into account, a single reference model is employed in the present work to improve the simplicity and hence applicability of the control method.

2) In this scheme, the therapist/slave only tracks the deviation of the patient/master from the moving target's trajectory and not the total patient's limb trajectory. In other words, the slave robot under the therapist's hand only follows the motion deviation of the master robot generated as impedance-based flexibility in response to the patient forces. This feature can reduce the therapist's movements and consequently, his fatigue in comparison with previous bilateral controllers [20, 21, 24, 32, 33, 46, 48] that generated the same trajectory for the master and slave robots (patient and therapist). Implementing the proposed control method, the therapist can sense the patient's deviations from the target trajectory directly and intuitively. On the other hand, the patient-therapist force reflection performance is achieved in the proposed strategy (when the therapist reduces the patient deviation to zero) similar to the force tracking performance in previous bilateral control

strategies [20, 21, 24, 32, 33, 46]. As a result, the therapist perceives similar haptic force feedback to the ones sensed in previous teleoperation methods, but the therapist has a smaller motion trajectory (only patient deviation) compared with the ones (total patient trajectory) tracked in previous strategies [20, 21, 24, 32, 33, 46]. Therefore, the therapist fatigue can be reduced by employing the proposed bilateral control strategy for a robotic tele-rehabilitation system since the therapist's hand does not have a large motion during applying assistive forces (which are transmitted to the patient).

3) Two sources of haptics-based assistance for following the moving target are provided to the patient using the adjustable impedance elements (spring, damper and mass) and the force applied by the therapist during cooperation with the patient. If the patient cannot follow the moving target and has a deviation, the impedance model provides a restoring force toward the target in proportion to the patient's deviation from the target's trajectory. Moreover, the therapist can intervene in the patient's trajectory by applying forces to the slave robot in order to amend the level of assistance provided to the patient via the master robot. These assistive forces are perceived by the patient as the haptic feedback, which can also be modified by adjustment of a force scaling factor.

4) The proposed desired impedance model can be adjusted based on the patient's symptoms and disabilities. Accordingly, two cases of impedance adjustment for patients suffering from insufficient actuation of muscles and from considerable tremors are presented.

5) Two different strategies are defined for mapping the therapist's and patient's motions and forces. In the first strategy, the therapist and patient workspaces are defined in the same Cartesian coordinates. The second strategy is designed such that the patient/master motion in the Normal-Tangential (N-T) coordinates with respect to the moving target trajectory is mapped to the Cartesian coordinates and then reflected to the therapist via the slave robot.

6) Implementing a stable impedance model and proving the Lyapunov-based stability of the multi-DOF tele-robotic system in the presence of various modeling uncertainties enhance the patient's and therapist's safety. Note that patient safety is highly important in robotic tele-rehabilitation systems and other physical human-robot interactions [14].

7) A new nonlinear bilateral adaptive controller is presented such that tracking convergence of the master and slave trajectories to their corresponding desired trajectories is proven using a Lyapunov-based framework. Note that the desired patient/master trajectory is obtained from the response of the impedance model, while the desired therapist/slave trajectory is equal to the patient's deviation from the target's trajectory as described in Sec. 2.2 and 2.3, respectively. Also, the robustness of the proposed bilateral adaptive controller against parametric (structured) and non-parametric (unstructured) uncertainties in the nonlinear teleoperation system is guaranteed by employing two types of adaptation laws, each for one type of uncertainty.

These features of the proposed bilateral impedance-based controller are useful for tele-rehabilitation applications using telerobotic systems. The rest of this paper is organized as follows. The desired objectives of the proposed assist-as-needed robotic tele-rehabilitation strategy are presented in Sec. 2. The scaling feature, and the master and slave robots control objectives are described in Sec. 2.1, Sec. 2.2 and Sec. 2.3, respectively. The impedance adjustments for patients with the low capability of force generation and with considerable tremors are introduced in Sec. 2.4 and Sec. 2.5, respectively. Two cases of force/motion mapping between the patient and therapist are introduced in Sec. 2.6. The safety of the patient and therapist is discussed in Sec. 2.7. In Sec. 3, the nonlinear dynamics of the multi-DOF telerobotic system for tele-rehabilitation is presented. Details of the nonlinear bilateral robust adaptive control method are proposed in Sec. 4. The stability and tracking convergence proof, together with two types of adaptation laws, are provided in Sec. 5 using the Lyapunov method. Comprehensive experimental results of the proposed strategy are reported and discussed in Sec. 6 concluding remarks are mentioned in Sec. 7.

## 2. The Assist-as-needed Robotic Tele-rehabilitation Strategy

In assistive rehabilitation scenarios, the patient is aided to perform a desired task like tracking a target. The level of this assistance can be chosen based on the stage of the rehabilitation process and the patient's improvement and engagement [5]. This assistance has been provided using the impedance control method [34] in rehabilitation systems with one robot manipulator [11].

In our assist-as-needed tele-rehabilitation strategy, a physical collaboration between the therapist and the patient is performed via a multi-DOF master-slave telerobotic system. The combination of the patient's and therapist's forces specifies the desired patient's trajectory. Therefore, the therapist can intervene and adjust the patient's trajectory by applying forces during the tele-rehabilitation process. The sources of assistance realized for the patient during the movement therapy and impedance parameters' adjustments based on the patient's disabilities and characteristics are introduced in the next sections.

In the proposed assist-as-needed tele-rehabilitation strategy, a desired reference impedance model is defined for the telerobotic system, where the patient-master interaction force $\mathbf{f}_{pa}$ and the scaled therapist-slave interaction force $\alpha_{\mathrm{f}}\mathbf{f}_{th}$ are inputs of this model. The output response trajectory (characterized by $\mathbf{x}_{des_m}$, $\dot{\mathbf{x}}_{des_m}$ and $\ddot{\mathbf{x}}_{des_m}$) of this impedance model is transmitted to and tracked by the master robot using its position controller. Also, the scaled position $\alpha_{\mathrm{p}}\mathbf{x}_m$, velocity $\alpha_{\mathrm{p}}\dot{\mathbf{x}}_m$ and acceleration $\alpha_{\mathrm{p}}\ddot{\mathbf{x}}_m$ of the master robot (or the patient's arm), and the scaled trajectory of the moving target to be followed by the patient ($\alpha_{\mathrm{p}}\mathbf{x}_{tar}$, $\alpha_{\mathrm{p}}\dot{\mathbf{x}}_{tar}$ and $\alpha_{\mathrm{p}}\ddot{\mathbf{x}}_{tar}$) are transmitted to the slave robot's controller. These concepts and transmitted signals are schematically shown in Fig. 1. Note that the moving target trajectory ($\mathbf{x}_{tar}$) can be designed based on the common daily movements and/or other therapeutic exercises chosen due to the therapist's opinion.

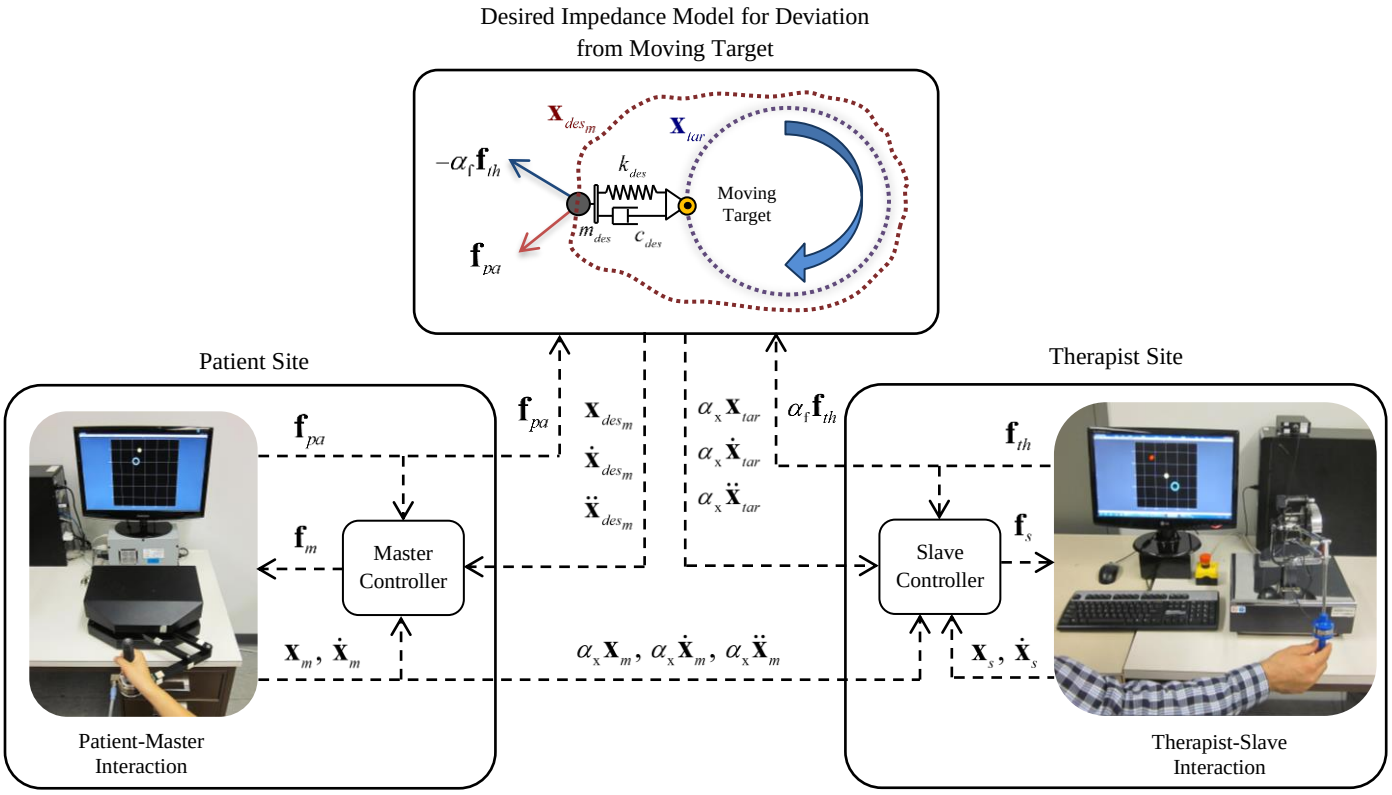


Fig. 1. Concepts of the proposed assistive tele-rehabilitation strategy with the patient-therapist cooperation defined via the desired impedance model.

As shown in Fig. 1, the trajectories of the master robot (or the patient's arm) and the target are scaled by $\alpha_{\mathrm{x}}$ for transmission to the slave controller. The therapist-slave interaction force $\mathbf{f}_{th}$ is also scaled by $\alpha_{\mathrm{f}}$ for transmission to the desired impedance model. Therefore, we have:

$$\mathbf{x}_{m_{scaled}} = \alpha_{\mathrm{x}}\,\mathbf{x}_m\,,\quad \mathbf{x}_{tar_{scaled}} = \alpha_{\mathrm{x}}\,\mathbf{x}_{tar}\,,\quad \mathbf{f}_{th_{scaled}} = \alpha_{\mathrm{f}}\,\mathbf{f}_{th} \quad (1)$$

The above position scaling feature is useful when the patient's arm deviation from the target $(\mathbf{x}_m - \mathbf{x}_{tar})$ is desired to be scaled up or down before tracking by the slave robot (or the therapist' hand). For instance, it may be suitable to use $\alpha_{\mathrm{x}} > 1$ such that the therapist can sense an amplified version of the small patient's deviation from the target. Also, to increase or decrease the therapist's influence on the response of the impedance model and consequently, the patient/master trajectory, the force scaling factor $\alpha_{\mathrm{f}}$ can be adjusted. For example, it may be desirable to have $\alpha_{\mathrm{f}} > 1$ in order to grant more authority to the therapist's force $\alpha_{\mathrm{f}}\mathbf{f}_{th}$ in comparison with the patient's force $\mathbf{f}_{pa}$ in the desired impedance model.

### 2.1. Master Robot Control Objective

The concept of impedance control in human-robot interactions and robotic rehabilitation in terms of displaying virtual appropriate mechanical elements (mass, damper and spring) by the robot to the human has been investigated and advanced in previous studies [11, 34-37]. In this research, The desired reference impedance model proposed below presents a cooperative behavior for the patient and the therapist in tracking the moving target's trajectory. This impedance model is defined as a dynamical relationship between a linear combination of the interaction force $\mathbf{f}_{pa}$ applied from the patient's arm to the master and the interaction force $\mathbf{f}_{th}$ applied from the slave to the therapist, and the desired master/patient deviation from the target trajectory $(\mathbf{x}_{des_m} - \mathbf{x}_{tar})$ as

$$\begin{aligned} m_{des}(\ddot{\mathbf{x}}_{des_m} - \ddot{\mathbf{x}}_{tar}) + c_{des}(\dot{\mathbf{x}}_{des_m} - \dot{\mathbf{x}}_{tar}) \\ + k_{des}(\mathbf{x}_{des_m} - \mathbf{x}_{tar}) = \mathbf{f}_{pa} - \alpha_{\mathrm{f}}\,\mathbf{f}_{th} \end{aligned} \quad (2)$$

Here, $\mathbf{x}_{tar}$ is the position trajectory of the moving target that is equal to the desired master robot's trajectory $\mathbf{x}_{des_m}$ in the absence of interaction forces (when $\mathbf{f}_{pa} = \mathbf{f}_{th} = 0$) based on Eq. (2). $k_{des}$, $c_{des}$ and $m_{des}$ are the desired virtual stiffness, damping and mass parameters of the reference impedance model, respectively. Note that in order to have different impedance characteristics in different directions of the motion space, these parameters can be replaced by matrices. The control objective of the master robot is tracking the response of the impedance model (2), i.e., $\mathbf{x}_m \to \mathbf{x}_{des_m}$. Once the master robot's controller achieves this objective, the collaboration of the patient and the therapist happens by applying forces to the master and the slave, respectively, such that the patient's deviation from the target position is adjusted based on Eq. (2).

Therefore, two adjustable sources of assistance are supplied to the patient based on Eq. (2), while following the moving target trajectory: a) The impedance elements $k_{des}$, $c_{des}$ and $m_{des}$ modulate the level of assistance delivered to the patient when moving the master toward the target trajectory. As the patient's deviation from the target trajectory $(\mathbf{x}_{des_m} - \mathbf{x}_{tar})$ increases, the magnitude of assistive force generated by the impedance model (2) increases, which is proportional to the values of the impedance parameters $k_{des}$, $c_{des}$ and $m_{des}$. Since the patient is aided more when he moves this limb farther from the target's position, this rehabilitation strategy is called "assist-as-needed". b) The scaled force $\alpha_{\mathrm{f}}\mathbf{f}_{th}$ of the therapist applied online to the slave robot can also assist the patient in tracking the target's trajectory regarding Eq. (2). As a result, the therapist intervenes in the patient's therapy exercises through modifying the haptic force feedback reflected to the master robot.

Moreover, as the impedance parameters ($k_{des}$, $c_{des}$ and $m_{des}$) decrease, the assistive force sensed by the patient decreases for a given deviation from the target $(\mathbf{x}_{des_m} - \mathbf{x}_{tar})$ based on Eq. (2), i.e., the patient's limb is less forcefully attracted to the target's position. This decrease in the assistance level can be adjusted

by the therapist before each trial in reaction to the patient's improvement in tracking the target. Also, the therapist adjusts his interaction force $\mathbf{f}_{th}$ during each trial.

It is worth noting that one impedance model (2) is utilized in this work to facilitate the above-mentioned beneficial characteristics in robotic rehabilitation; however, in the previous works on tele-rehabilitation [45-48], two or more models were needed. For this purpose, the combination of the patient and the therapist forces generates the desired patient deviation from a moving target using the proposed reference impedance model. This implies that multiple impedance models in the previous studies [45-48] are summed up in one reference model for the simplicity of the control design and its practical applicability in rehabilitation using a moving target.

### 2.2. Slave Robot Control Objective

The desired trajectory to be tracked by the slave robot is the scaled deviation $\alpha_x(\mathbf{x}_m - \mathbf{x}_{tar})$ of the master/patient from the target's position. Thus, the therapist, interacting with the slave robot, can easily recognize the patient's deviation and his motor deficiencies without moving along the target trajectory. This feature can reduce the therapist's movements and consequently his fatigue in comparison with previous bilateral controllers [20, 21, 24, 32, 33, 46, 48] that generated the same trajectory for the master and slave robots (i.e., patient and therapist).

Once the slave robot's position controller reaches its objective $\mathbf{x}_s \to \alpha_x(\mathbf{x}_m - \mathbf{x}_{tar})$, the therapist finds out the direction and also the magnitude of the patient's deviation from the target trajectory. Then, the therapist can adjust his force $\mathbf{f}_{th}$ and affect the patient's deviation based on the impedance model (2). Specifically, assuming the master trajectory has converged to its desired one (i.e., $\mathbf{x}_m \to \mathbf{x}_{des_m}$), if the therapist decides to decrease the patient's deviation from the target trajectory to zero, i.e., $(\mathbf{x}_m - \mathbf{x}_{tar}) \simeq (\mathbf{x}_{des_m} - \mathbf{x}_{tar}) \to 0$, he should apply the appropriate force $\mathbf{f}_{th}$ to the slave end-effector such that the master robot's position converges to the target. Since the slave robot's controller pursues tracking the patient's deviation, the slave end-effector under the therapist's hand will also converge to the origin as $\mathbf{x}_s \to \alpha_x(\mathbf{x}_m - \mathbf{x}_{tar}) \to 0$.

Therefore, as the therapist-patient collaboration leads to the convergence of the patient/master trajectory to the moving target's one, the therapist/slave trajectory will approach the origin. In this case, the left side of Eq. (2) in terms of $(\mathbf{x}_{des_m} - \mathbf{x}_{tar})$ has converged to the zero; therefore, the right side should also converge to zero: $(\mathbf{f}_{pa} - \alpha_f \mathbf{f}_{th}) \to 0$. Consequently, the therapist perceives and overcomes the scaled patient's force, i.e., $\mathbf{f}_{th} \to (1/\alpha_f)\mathbf{f}_{pa}$, for having the patient follows the target's trajectory without actually moving together with the patient, which would have resulted in a reduction of the therapist's fatigue. As a result, the therapist perceives similar haptic force feedback to the ones sensed in previous teleoperation strategies, while he has a smaller motion trajectory (the patient deviation) in comparison with the one (the total patient trajectory) tracked in previous strategies [20, 21, 24, 32, 33, 46].

According to the mentioned objectives in Sec. 2.1 and Sec. 2.2, a bilateral coupling is realized between the master and slave robots in terms of the position synchronization and force reflection in the conceptual design of the proposed controller like previous bilateral control strategies. Although, the defined impedance model (2) operates as a mediator for force reflection from slave to master. Furthermore, the deviation of the master trajectory (from a moving target) is treated as the desired position for the slave response instead of tracking the total master trajectory.

Although the patient and therapist can be in the same clinical setting, employing a master-slave telerobotic system and proposed control strategy enables the therapist to intervene minimally and apply a portion of the required assistive force to the slave robot in order to correct the trajectory deviation of the patient on the master site. The other source of assistance is provided by the defined impedance model, as explained in Sec. 2.1.

### 2.3. Impedance Adjustment for Patients with Low Capability of Force Generation

People with disabilities may suffer from insufficient actuation forces of muscles in reaching tasks. For example, post-stroke patients may not be able to move their limbs to the desired target location successfully. The impedance model (2) should be adjusted appropriately for these individuals to assist them in tracking a moving target. For this purpose, the impedance parameters $k_{des}$, $c_{des}$ and $m_{des}$ in (2) are chosen to have large values such that the patient's deviation from the target $(\mathbf{x}_m - \mathbf{x}_{tar})$ decreases for a given patient's force $\mathbf{f}_{pa}$. In this case, a powerful enough assistive force applied to the master robot is generated by the master robot's controller to absorb the patient's limb to the moving target trajectory.

### 2.4. Impedance Adjustment for Patients with Tremors

Patients having Parkinson's disease (PD), cerebral palsy (CP), multiple sclerosis (MS) or stroke may experience oscillatory tremors in the actions, intentions and purposeful movements of their limbs [49, 50]. The frequency range of these rhythmic involuntary movements is $3-6$ Hz [49, 50].

#### *2.4.1. Adjustment for Tremor Filtration*

Using the proposed impedance-based control strategy, the patient tremor (high-frequency movement) can be filtered out such that it affects neither the patient's motions nor the therapist's motions. For this purpose, the reference impedance model (2) should be adjusted such that its response $\mathbf{x}_{des_m}$ is not affected by the high-frequency portion $\mathbf{f}_{pa_{trem}}$ of the patient's interaction force $\mathbf{f}_{pa} = \mathbf{f}_{pa_{LF}} + \mathbf{f}_{pa_{trem}}$.

A suitable adjustment for the impedance model (2) as a second-order differential equation is that its cut-off frequency ($\approx \omega_n = \sqrt{k_{des}/m_{des}}$) is several times smaller than the minimum tremor frequency ($\omega_{trem_{\min}}$). In Fig. 2, the magnitude Bode diagram of the desired impedance model shows that if $\omega_n \ll \omega_{trem}$, the involuntary tremor-related high-frequency portion of the patient's force is attenuated significantly. Therefore, due to (2) and based on the $-40$ dB/decade slope of the Bode plot in frequencies higher than the natural (cut-off) frequency $\omega_n$, the magnitude of the desired impedance model's response with respect to the tremor portion of the patient's force is $|\mathbf{X}_{des_{trem}}| \le (\omega_{trem_{\min}}/\omega_n)^2 |\mathbf{F}_{pa\,trem}/k_{des}|$.

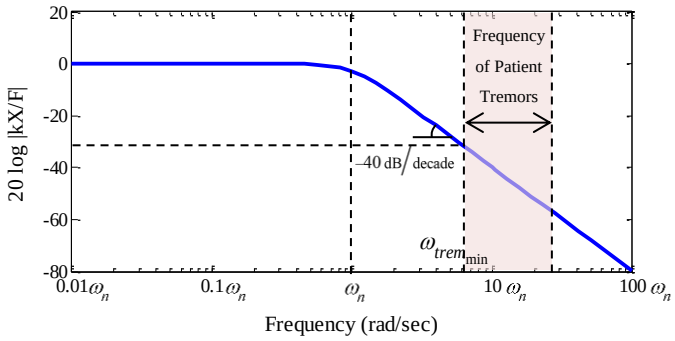


Fig. 2. The magnitude Bode diagram of the under-damped ($\xi = c_{des}/2\sqrt{m_{des}k_{des}} = 0.7$) linear second order system with natural frequency of $\omega_n = \sqrt{k_{des}/m_{des}}$ for filtration of the patient's limb tremor. The oscillatory tremors are considered to have a minimum frequency of $\omega_{trem_{\min}}$.

Having this adjustment, the master robot's trajectory $\mathbf{x}_m$ that tracks $\mathbf{x}_{des_m}$ is smooth and tremor-free, and the patient can perform the rehabilitation task with suppression of his involuntary tremors. Thus, the therapist's motion is also not affected by the patient's tremor as the slave robot tracks the difference between the smooth master/patient and target trajectories, i.e., $\mathbf{x}_s \to \alpha_x(\mathbf{x}_m - \mathbf{x}_{tar})$. Such elimination of patient tremors reduces the therapist's fatigue.

#### *2.4.2. Adjustment for Tremor Reflection*

In some instances, it may be desired that the patient moves with his own tremors during the interaction with the master robot for tele-rehabilitation in order to monitor his free natural motions. In such cases, the tremor-related high-frequency portion of the patient force should not be filtered out via the impedance model (2), unlike the adjustment presented in Sec.

2.4.1. Therefore, the patient's limb is not restricted to have a smooth trajectory without his tremor movements. For this purpose, the natural frequency of the impedance model should be chosen larger than the patient's tremor frequencies: $\omega_n \geq \omega_{trem}$ (unlike the case in Sec. 2.4.1). In this case, the therapist can also sense the patient's tremors via the haptic perception provided by the telerobotic system. In other words, the slave robot tracks the patient's position deviation from the target that includes tremor-related high-frequency movements.

According to the presented discussion in Sec. 2.4.1 and Sec. 2.4.2, the assistive tele-rehabilitation process can be performed using the proposed strategy with and without tremor filtration for the PD, CP, MS and stroke patients.

## 2.5. Two Cases of Force-motion Mapping Between the Patient and Therapist

In the proposed tele-rehabilitation system, two cases of mapping for the position and force data are brought forward between the patient/master and the therapist/slave. The first one is defined in the Cartesian space, and the second one is presented as a mapping between the Cartesian and Normal-Tangential coordinates. The therapist can select each of these mappings based on his preference and/or the direction of patient's deviations.

Note that the proposed assistive tele-rehabilitation strategy and corresponding nonlinear bilateral controller are designed generally for *n*-DOF master and slave robots in this paper. Thus, the robots' end-effectors can move in three-dimensional space; however, the mapping between the Cartesian and the Normal-Tangential (N-T) coordinates are described and illustrated (Fig. 3) in two dimensional (planar) space in this section for the simplicity.

### *2.5.1. Cartesian to Cartesian Mapping*

In the first mapping, the position deviation of the patient/master with respect to the moving target in the Cartesian space is provided for the therapist in the same space using the slave robot's controller. As shown in Fig. 3a, the Cartesian direction of the patient's deviation $(\mathbf{x}_m - \mathbf{x}_{tar})$ is the same as the scaled and mapped trajectory tracked by the therapist/slave: $\mathbf{x}_s \rightarrow \alpha_{\mathrm{x}}(\mathbf{x}_m - \mathbf{x}_{tar})_{Map}$. Also, the mapped therapist's force $\mathbf{f}_{th_{Map}}$ in the Cartesian coordinates is used in the impedance model (2), the same as the patient's force $\mathbf{f}_{pa}$.

### *2.5.2. Normal-Tangential to Cartesian Mapping*

The second case of mapping is defined such that the patient's position in the Normal-Tangential (N-T) coordinates is mapped to the therapist's position in the Cartesian coordinates, as illustrated in Fig. 3b. In this case, the Normal-Tangential coordinates rotate with respect to the moving target's location in its path, such that the normal $x$ and tangential $y$ axes are always perpendicular and parallel to the concurrent tangent of the target's trajectory, respectively. The therapist's force should also be mapped ($\mathbf{f}_{th_{Map}}$) from the Cartesian to the Normal-Tangential coordinates before being used in the impedance model (2).

Having this type of mapping, the therapist can guide the patient forward and backward along the target trajectory by applying force $\mathbf{f}_{th}$ toward $+y$ and $-y$ directions, respectively, in the Cartesian coordinates (Fig. 3b). Similarly, the therapist can push the patient toward the inside or outside of the arc of moving target's path via applying the force in $+x$ and $-x$ directions (Fig. 3b). Moreover, the scaled patient's position deviation with respect to the moving target is contrariwise mapped to the slave/therapist's desired position: $\mathbf{x}_s \rightarrow \alpha_{\mathrm{x}}(\mathbf{x}_m - \mathbf{x}_{tar})_{Map}$. In other words, the patient's deviation to the front and back of the target's position in its desired path will move the therapist's hand in the $+y$ and $-y$ directions, respectively, in the Cartesian coordinates. Also, the patient's deviation toward the inside or outside of the target's trajectory will push the therapist into $+x$ or $-x$ directions, respectively.

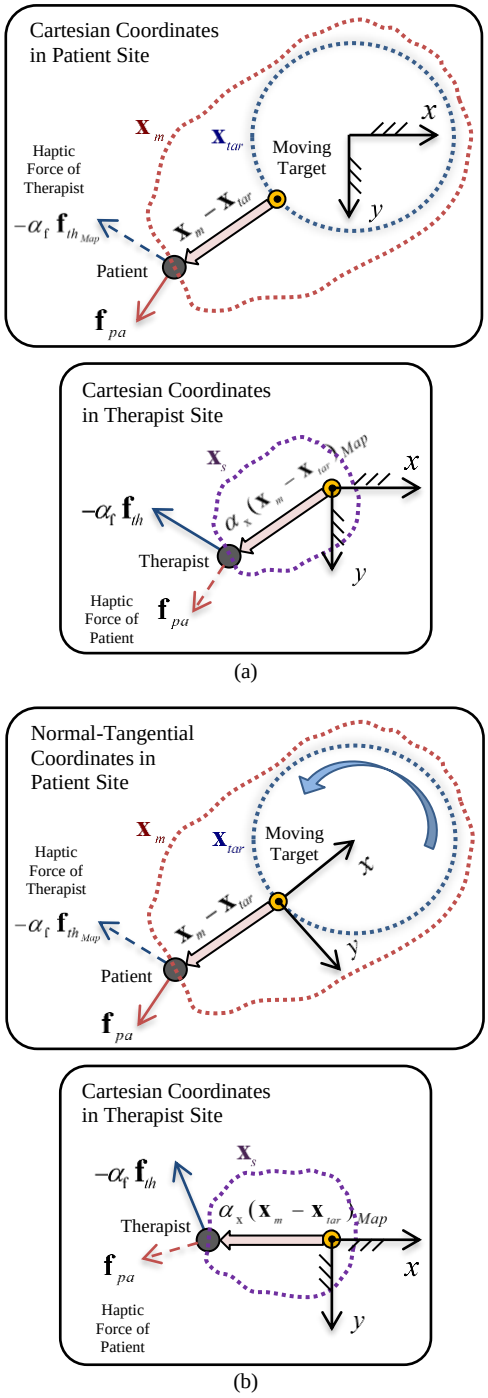


Fig. 3. Different cases of force-motion mapping between the patient and therapist: (a) Cartesian to Cartesian Mapping, and (b) Normal-Tangential to Cartesian Mapping.

### 2.6. Patient's and Therapist's Safety

The desired impedance model (2) is a stable second-order differential equation if positive values are employed for the impedance parameters $k_{des}$, $c_{des}$ and $m_{des}$. In other words, bounded input forces of the patient $\mathbf{f}_{pa}$ and therapist $\mathbf{f}_{th}$ will not generate unbounded impedance response $(\mathbf{x}_{des_m} - \mathbf{x}_{tar})$ based on Eq. (2). Therefore, using a bounded trajectory $\mathbf{x}_{tar}$ for the moving target, $\mathbf{x}_{des_m}$ will be bounded as the desired trajectory tracked by the master robot ($\mathbf{x}_m \to \mathbf{x}_{des_m}$). Also, due to the boundedness of $\mathbf{x}_m$ and $\mathbf{x}_{tar}$, the scaled patient's deviation from the target's position becomes bounded as the desired trajectory tracked by the slave robot $\mathbf{x}_s \to \alpha_x(\mathbf{x}_m - \mathbf{x}_{tar})$. Moreover, the master and slave tracking convergence to their desired trajectories are obtained using a nonlinear bilateral controller (Sec. 4), as proven in Sec. 5 through a rigorous Lyapunov-based stability analysis. Accordingly, the master and slave robots have bounded trajectories in response to the bounded interaction forces applied by the patient $\mathbf{f}_{pa}$ and therapist $\mathbf{f}_{th}$. This characteristic of the proposed robotic tele-rehabilitation systems based on the proposed impedance control framework significantly enhances the safety of the patient and therapist during their physical interactions with the master and slave robots, respectively.

## 3. Nonlinear Multi-DOF Telerobotic System for Tele-Rehabilitation

The nonlinear dynamics of a multi-DOF tele-rehabilitation system including the master and slave robot manipulators is presented in the Cartesian space as [51]

$$\mathbf{M}_{\mathbf{x},m}(\mathbf{q}_m)\ddot{\mathbf{x}}_m + \mathbf{C}_{\mathbf{x},m}(\mathbf{q}_m,\dot{\mathbf{q}}_m)\dot{\mathbf{x}}_m + \mathbf{G}_{\mathbf{x},m}(\mathbf{q}_m) + \mathbf{F}_{\mathbf{x},m}(\dot{\mathbf{q}}_m) = \mathbf{f}_m + \mathbf{f}_{pa} + \mathbf{u}_{\mathbf{x},m} \quad (3)$$

$$\mathbf{M}_{\mathbf{x},s}(\mathbf{q}_s)\ddot{\mathbf{x}}_s + \mathbf{C}_{\mathbf{x},s}(\mathbf{q}_s,\dot{\mathbf{q}}_s)\dot{\mathbf{x}}_s + \mathbf{G}_{\mathbf{x},s}(\mathbf{q}_s) + \mathbf{F}_{\mathbf{x},s}(\dot{\mathbf{q}}_s) = \mathbf{f}_s - \mathbf{f}_{th} + \mathbf{u}_{\mathbf{x},s} \quad (4)$$

where $\mathbf{q}_m$ and $\mathbf{q}_s$ are the joint positions, $\mathbf{x}_m$ and $\mathbf{x}_s$ are the Cartesian positions of the end-effectors, $\mathbf{M}_{\mathbf{x},m}(\mathbf{q}_m)$ and $\mathbf{M}_{\mathbf{x},s}(\mathbf{q}_s)$ are the inertia or mass matrices, $\mathbf{C}_{\mathbf{x},m}(\mathbf{q}_m,\dot{\mathbf{q}}_m)$ and $\mathbf{C}_{\mathbf{x},s}(\mathbf{q}_s,\dot{\mathbf{q}}_s)$ consist of the centrifugal and Coriolis terms, $\mathbf{G}_{\mathbf{x},m}(\mathbf{q}_m)$ and $\mathbf{G}_{\mathbf{x},s}(\mathbf{q}_s)$ are the gravity terms, $\mathbf{F}_{\mathbf{x},m}(\dot{\mathbf{q}}_m)$ and $\mathbf{F}_{\mathbf{x},s}(\dot{\mathbf{q}}_s)$ are the

friction forces, and $\mathbf{f}_m$ and $\mathbf{f}_s$ are the control forces from the actuators of the master and the slave robots, respectively. $\mathbf{f}_{pa}$ is the interaction force that the patient applies to the master's end-effector, and $\mathbf{f}_{th}$ is the interaction force that the slave end-effector applies to the therapist. The vectors of bounded (non-parametric) unstructured modeling uncertainties and/or bounded exogenous disturbances of the system are also denoted by $\mathbf{u}_{\mathbf{x},m}$ and $\mathbf{u}_{\mathbf{x},s}$ for the master and slave robots, respectively.

It is considered that the unstructured modeling uncertainties and/or disturbances are bounded, and there exist positive constants $\lambda_m$ and $\lambda_s$ such that

$$\left\|\mathbf{u}_{\mathbf{x},m}\right\|_\infty \le \lambda_m \ , \quad \left\|\mathbf{u}_{\mathbf{x},s}\right\|_\infty \le \lambda_s \tag{5}$$

The above inequalities indicate that the $j^{\text{th}}$ component of the master and slave non-parametric uncertainty vectors satisfies the following condition: $\left|\mathbf{u}_{\mathbf{x},m_j}\right| \le \lambda_m$ and/or $\left|\mathbf{u}_{\mathbf{x},s_j}\right| \le \lambda_s$.

The dynamics of the telerobotic system in the joint space and the transformation between the joint and Cartesian spaces are mentioned in Appendix.

Using the subscript $i = m$ for the master and $i = s$ for the slave, the dynamic matrices and vectors in (3) and (4) have the following properties [51-53]:

**Property 1.** The left side of (3) and (4) can be linearly parameterized as

$$\begin{aligned}\mathbf{M}_{\mathbf{x},i}(\mathbf{q}_i)\boldsymbol{\xi}_{\mathbf{1},i} + \mathbf{C}_{\mathbf{x},i}(\mathbf{q}_i,\dot{\mathbf{q}}_i)\boldsymbol{\xi}_{\mathbf{2},i} + \mathbf{G}_{\mathbf{x},i}(\mathbf{q}_i) + \mathbf{F}_{\mathbf{x},i}(\dot{\mathbf{q}}_i) \\ = \mathbf{R}_{\mathbf{x},i}(\xi_{1,i},\xi_{2,i},\mathbf{q}_i,\dot{\mathbf{q}}_i)\boldsymbol{\delta}_{\mathbf{x},i}\end{aligned} \tag{6}$$

where $\boldsymbol{\delta}_{\mathbf{x},i}$ is the vector of unknown parameters of each robot. The regressor matrix $\mathbf{R}_{\mathbf{x},i}$ contains the known functions of the vectors $\boldsymbol{\xi}_{\mathbf{1},i}$ and $\boldsymbol{\xi}_{\mathbf{2},i}$ [51].

**Property 2.** The matrix $\dot{\mathbf{M}}_{\mathbf{x},i} - 2\mathbf{C}_{\mathbf{x},i}$ is skew symmetric and the inertia matrix $\mathbf{M}_{\mathbf{x},i}$ is symmetric positive definite.

## 4. Nonlinear Bilateral Robust Adaptive Control Method

As mentioned earlier, the control objective of the master robot is tracking the response of the reference impedance model: $\mathbf{x}_m \to \mathbf{x}_{des_m}$, and the control objective of the slave robot is tracking the scaled deviation of the patient/master from the target trajectory: $\mathbf{x}_s \to \mathbf{x}_{des_s} = \alpha_{\mathrm{x}}(\mathbf{x}_m - \mathbf{x}_{tar})_{Map}$. These control objectives are achieved using the designed nonlinear bilateral controller in the presence of parametric (structured) and non-parametric (unstructured) uncertainties in the dynamic models of the master and slave robots. The conceptual block diagram of the proposed nonlinear bilateral robust adaptive controller is shown in Fig. 4 and its design is detailed in this section. Note that the forces of the patient and therapist ($\mathbf{f}_{pa}$ and $\mathbf{f}_{th}$) during their physical interaction with robots are measured using force sensors attached to the master and slave end-effectors, respectively.

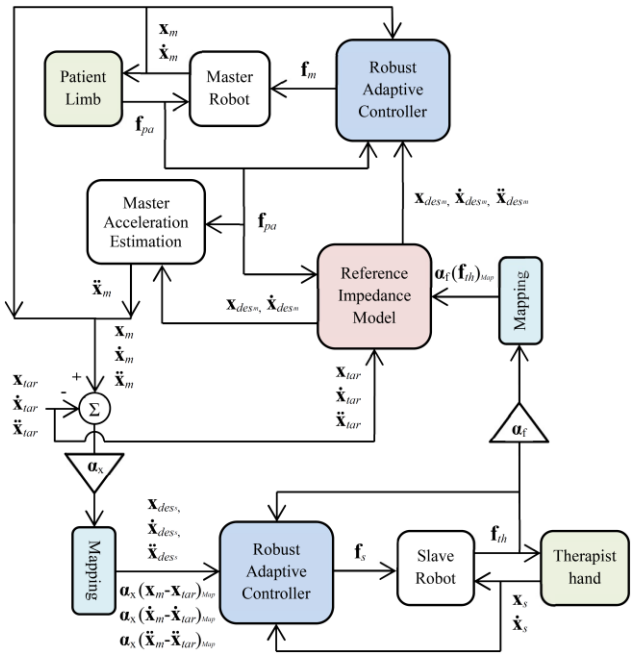


Fig. 4. The conceptual block diagram of the nonlinear bilateral robust adaptive controller for assistive tele-rehabilitation.

Accordingly, two nonlinear robust adaptive control laws are designed and presented for the master and slave robots. For this purpose, two sliding surfaces are introduced for the master and slave controllers as

$$\begin{aligned}\boldsymbol{\varepsilon}_m &= \dot{\tilde{\mathbf{x}}}_m + \beta_{1,m}\tilde{\mathbf{x}}_m + \beta_{2,m}\int_0^t \tilde{\mathbf{x}}_m\, dt\ ,\\ \boldsymbol{\varepsilon}_s &= \dot{\tilde{\mathbf{x}}}_s + \beta_{1,s}\tilde{\mathbf{x}}_s + \beta_{2,s}\int_0^t \tilde{\mathbf{x}}_s\, dt\end{aligned} \tag{7}$$

where $\tilde{\mathbf{x}}_m = \mathbf{x}_m - \mathbf{x}_{des_m}$, $\tilde{\mathbf{x}}_s = \mathbf{x}_s - \mathbf{x}_{des_s}$ are the position tracking errors of the master and slave robots with respect to their desired responses of $\mathbf{x}_{des_m}$ and $\mathbf{x}_{des_s}$. As mentioned before, $\mathbf{x}_{des_m}$ is the response of the desired impedance model (2) and $\mathbf{x}_{des_S} = \alpha_{\mathrm{x}}(\mathbf{x}_m - \mathbf{x}_{tar})_{Map}$ is the scaled and mapped patient-target position deviation. Also, $\beta_{1,m}$, $\beta_{2,m}$, $\beta_{1,s}$ and $\beta_{2,s}$ are four positive constant parameters to guarantee the stability of the three-term sliding surfaces (7), i.e. $\tilde{\mathbf{x}}_i \to 0$ as $\boldsymbol{\varepsilon}_i \to 0$. The reference velocities of the master and slave are defined based on Eq. (7) as

$$\begin{aligned}\dot{\mathbf{x}}_{ref,m} &= \dot{\mathbf{x}}_{des_m} - \beta_{1,m}\tilde{\mathbf{x}}_m - \beta_{2,m}\int_0^t \tilde{\mathbf{x}}_m\, dt\\ \dot{\mathbf{x}}_{ref,s} &= \dot{\mathbf{x}}_{des_S} - \beta_{1,s}\tilde{\mathbf{x}}_s - \beta_{2,s}\int_0^t \tilde{\mathbf{x}}_s\, dt\end{aligned} \tag{8}$$

As a result, the sliding surfaces (7) are represented as $\boldsymbol{\varepsilon}_m = \dot{\mathbf{x}}_m - \dot{\mathbf{x}}_{ref,m}$ and $\boldsymbol{\varepsilon}_s = \dot{\mathbf{x}}_s - \dot{\mathbf{x}}_{ref,s}$. Now, the nonlinear bilateral robust adaptive control laws for the master and slave end-effectors in the Cartesian space are designed as

$$\begin{aligned}\mathbf{f}_m = &-\beta_{3,m}\hat{\mathbf{M}}_{\mathbf{x},m}(\mathbf{q}_m)\boldsymbol{\varepsilon}_m + \hat{\mathbf{M}}_{\mathbf{x},m}(\mathbf{q}_m)\ddot{\mathbf{x}}_{ref,m}\\ &+\hat{\mathbf{C}}_{\mathbf{x},m}(\mathbf{q}_m,\dot{\mathbf{q}}_m)\dot{\mathbf{x}}_{ref,m} + \hat{\mathbf{G}}_{\mathbf{x},m}(\mathbf{q}_m) + \hat{\mathbf{F}}_{\mathbf{x},m}(\dot{\mathbf{q}}_m)\\ &-\mathbf{f}_{pa} - \hat{\gamma}_m\,\mathrm{sgn}(\boldsymbol{\varepsilon}_m)\end{aligned} \tag{9}$$

$$\begin{aligned}\mathbf{f}_S = &-\beta_{3,s}\hat{\mathbf{M}}_{\mathbf{x},s}(\mathbf{q}_s)\boldsymbol{\varepsilon}_s + \hat{\mathbf{M}}_{\mathbf{x},s}(\mathbf{q}_s)\ddot{\hat{\mathbf{x}}}_{ref,s}\\ &+\hat{\mathbf{C}}_{\mathbf{x},s}(\mathbf{q}_s,\dot{\mathbf{q}}_s)\dot{\mathbf{x}}_{ref,s} + \hat{\mathbf{G}}_{\mathbf{x},s}(\mathbf{q}_s) + \hat{\mathbf{F}}_{\mathbf{x},s}(\dot{\mathbf{q}}_s)\\ &+\mathbf{f}_{th} - \hat{\gamma}_s\,\mathrm{sgn}(\boldsymbol{\varepsilon}_s)\end{aligned} \tag{10}$$

where accent $\wedge$ denotes the estimated and/or updated values of the corresponding matrix, vector or scalar. It will be proven that $-\hat{\gamma}_m\,\mathrm{sgn}(\boldsymbol{\varepsilon}_m)$ and $-\hat{\gamma}_s\,\mathrm{sgn}(\boldsymbol{\varepsilon}_s)$ guarantee the robustness of the proposed bilateral controller against the bounded non-parametric (unstructured) uncertainties and/or disturbances $\mathbf{u}_{\mathbf{x},m}$ and $\mathbf{u}_{\mathbf{x},s}$, introduced in the telerobotic system's dynamics (3) and (4). Also, $\hat{\gamma}_m$ and $\hat{\gamma}_s$ are two varying robust gains that are intelligently updated via adaptation laws to overcome the bounds of non-parametric uncertainties (this will be proven in the Sec. 5).

Note that the acceleration of the master robot ($\ddot{\mathbf{x}}_m$) is required in the slave control law (10) that is defined in terms of $\ddot{\mathbf{x}}_{ref,s}$, which itself is a function of $\ddot{\mathbf{x}}_{des_S} = \alpha_{\mathrm{x}}(\ddot{\mathbf{x}}_m - \ddot{\mathbf{x}}_{tar})_{Map}$ based on Eq. (8). However, since the robot's acceleration measurement is challenging, $\ddot{\mathbf{x}}_m$ is estimated with a good accuracy when the master robot mimics the impedance model (2) by tracking convergence to its response: $\mathbf{x}_m \to \mathbf{x}_{des_m}$, $\dot{\mathbf{x}}_m \to \mathbf{x}_{des_m}$. In other words, the estimation of the master end-effector acceleration $\ddot{\mathbf{x}}_m$ is determined from (2) as

$$\begin{aligned}\ddot{\mathbf{x}}_m \simeq\ & \ddot{\mathbf{x}}_{tar} + m_{des}^{-1}\left(\mathbf{f}_{pa} - \alpha_{\mathrm{f}}\mathbf{f}_{th}\right)\\ & - m_{des}^{-1}\,c_{des}\,(\dot{\mathbf{x}}_{des_m} - \dot{\mathbf{x}}_{tar}) - m_{des}^{-1}\,k_{des}\,(\mathbf{x}_{des_m} - \mathbf{x}_{tar})\end{aligned} \tag{11}$$

Thus, when the master's trajectory $\mathbf{x}_m$ converges to the desired impedance model's response $\mathbf{x}_{des_m}$, the accuracy of (11) in estimating the master's acceleration increases. For employing (11), the measured patient's force $\mathbf{f}_{pa}$ together with the master robot's trajectory data ($\mathbf{x}_m$ and $\dot{\mathbf{x}}_m$) should be transferred from the patient/master site toward the therapist/slave site (instead of transmitting $\ddot{\mathbf{x}}_m$ together with $\mathbf{x}_m$ and $\dot{\mathbf{x}}_m$), as illustrated in Fig. 4.

The motor torques of robots (control laws in the joint space) are also presented in Appendix. Using Property 1, the control laws (9) and (10) are simplified as

$$\mathbf{f}_m = \mathbf{R}_{\mathbf{x},m}\hat{\boldsymbol{\delta}}_{\mathbf{x},m} - \mathbf{f}_{pa} - \hat{\gamma}_m\,\mathrm{sgn}(\boldsymbol{\varepsilon}_m) \tag{12}$$

$$\mathbf{f}_s = \mathbf{R}_{\mathbf{x},s}\hat{\boldsymbol{\delta}}_{\mathbf{x},s} + \mathbf{f}_{th} - \hat{\gamma}_s\,\mathrm{sgn}(\boldsymbol{\varepsilon}_s) \tag{13}$$

where $\mathbf{R}_{\mathbf{x},m}$ and $\mathbf{R}_{\mathbf{x},s}$ are the regressor matrices introduced in (6) in terms of these known vectors:

$$\begin{aligned} \boldsymbol{\xi}_{\mathbf{1},m} &= -\beta_{3,m}\ \boldsymbol{\varepsilon}_m + \ddot{\mathbf{x}}_{ref,m}, \quad \boldsymbol{\xi}_{\mathbf{2},m} = \dot{\mathbf{x}}_{ref,m} \\ \boldsymbol{\xi}_{\mathbf{1},s} &= -\beta_{3,s}\ \boldsymbol{\varepsilon}_s + \ddot{\mathbf{x}}_{ref,s}, \quad \boldsymbol{\xi}_{\mathbf{2},s} = \dot{\mathbf{x}}_{ref,s} \end{aligned} \tag{14}$$

In order to obtain the closed-loop dynamics of the master and slave robots, the control laws (9) and (10) are substituted in the dynamics (3) and (4) of the tele-robotic system. This turns out after some simplifications as

$$\begin{aligned} \mathbf{M}_{\mathbf{x},m}(\dot{\boldsymbol{\varepsilon}}_m + \beta_{3,m}\boldsymbol{\varepsilon}_m) + \mathbf{C}_{\mathbf{x},m}\boldsymbol{\varepsilon}_m = \\ \mathbf{R}_{\mathbf{x},m}\tilde{\boldsymbol{\delta}}_{\mathbf{x},m} + \mathbf{u}_{\mathbf{x},m} - \hat{\gamma}_m\,\mathrm{sgn}(\boldsymbol{\varepsilon}_m) \end{aligned} \tag{15}$$

$$\begin{aligned} \mathbf{M}_{\mathbf{x},s}(\dot{\boldsymbol{\varepsilon}}_s + \beta_{3,s}\boldsymbol{\varepsilon}_s) + \mathbf{C}_{\mathbf{x},s}\boldsymbol{\varepsilon}_s = \\ \mathbf{R}_{\mathbf{x},s}\tilde{\boldsymbol{\delta}}_{\mathbf{x},s} + \mathbf{u}_{\mathbf{x},s} - \hat{\gamma}_s\,\mathrm{sgn}(\boldsymbol{\varepsilon}_s) \end{aligned} \tag{16}$$

where $\tilde{\boldsymbol{\delta}}_{\mathbf{x},m} = \hat{\boldsymbol{\delta}}_{\mathbf{x},m} - \boldsymbol{\delta}_{\mathbf{x},m}$ and $\tilde{\boldsymbol{\delta}}_{\mathbf{x},s} = \hat{\boldsymbol{\delta}}_{\mathbf{x},s} - \boldsymbol{\delta}_{\mathbf{x},s}$ are the parameter estimation errors of the master and slave dynamics, respectively.

## 5. Stability, Tracking Convergence and Adaptation Laws

The Lyapunov stability of the proposed robotic tele-rehabilitation system and tracking convergence of the master and slave trajectories to their desired responses ($\mathbf{x}_m \to \mathbf{x}_{des_m}$ and $\mathbf{x}_s \to \mathbf{x}_{des_s}$) are proven in this section. The robustness of the controlled teleoperation system against parametric and bounded non-parametric uncertainties is also guaranteed via defining and employing two types of adaptation laws.

### 5.1. Lyapunov Function

For the above-mentioned purposes, a positive-definite candidate Lyapunov function is defined as:

$$\begin{aligned} V(t) = \frac{1}{2}\big(&\boldsymbol{\varepsilon}_m^T\mathbf{M}_{\mathbf{x},m}\boldsymbol{\varepsilon}_m + \tilde{\boldsymbol{\delta}}_{\mathbf{x},m}^T\boldsymbol{\Psi}_m^{-1}\tilde{\boldsymbol{\delta}}_{\mathbf{x},m} + (1/\rho_m)(\hat{\gamma}_m - \lambda_m)^2 \\ &+ \boldsymbol{\varepsilon}_s^T\mathbf{M}_{\mathbf{x},s}\boldsymbol{\varepsilon}_s + \tilde{\boldsymbol{\delta}}_{\mathbf{x},s}^T\boldsymbol{\Psi}_s^{-1}\tilde{\boldsymbol{\delta}}_{\mathbf{x},s} + (1/\rho_s)(\hat{\gamma}_s - \lambda_s)^2\big) \end{aligned}$$

(17)

where $\lambda_m$ and $\lambda_s$ are the unknown upper bounds of the unstructured (non-parametric) modeling uncertainties, introduced in (5). $\boldsymbol{\Psi}_m$ and $\boldsymbol{\Psi}_s$ are symmetric positive-definite constant matrices as gains of the first adaptation law for updating the estimation of uncertain master and slave parameters $\hat{\boldsymbol{\delta}}_{\mathbf{x},m}$ and $\hat{\boldsymbol{\delta}}_{\mathbf{x},s}$. $\rho_m$ and $\rho_s$ are positive constants acting as gains of the second adaptation law for updating the robust gains $\hat{\gamma}_m$ and $\hat{\gamma}_s$ of the controller. These two types of adaptation laws are defined in Sec. 5.2 and Sec. 5.3.

Now, the time derivative of the Lyapunov function (17) is determined as

$$\begin{aligned} \dot{V}(t) = &\frac{1}{2}\boldsymbol{\varepsilon}_m^T\dot{\mathbf{M}}_{\mathbf{x},m}\boldsymbol{\varepsilon}_m + \boldsymbol{\varepsilon}_m^T\mathbf{M}_{\mathbf{x},m}\dot{\boldsymbol{\varepsilon}}_m \\ &+ \dot{\tilde{\boldsymbol{\delta}}}_{\mathbf{x},m}^T\boldsymbol{\Psi}_m^{-1}\tilde{\boldsymbol{\delta}}_{\mathbf{x},m} + (1/\rho_m)(\hat{\gamma}_m - \lambda_m)\dot{\hat{\gamma}}_m \\ &+ \frac{1}{2}\boldsymbol{\varepsilon}_s^T\dot{\mathbf{M}}_{\mathbf{x},s}\boldsymbol{\varepsilon}_s + \boldsymbol{\varepsilon}_s^T\mathbf{M}_{\mathbf{x},s}\dot{\boldsymbol{\varepsilon}}_s \\ &+ \dot{\tilde{\boldsymbol{\delta}}}_{\mathbf{x},s}^T\boldsymbol{\Psi}_s^{-1}\tilde{\boldsymbol{\delta}}_{\mathbf{x},s} + (1/\rho_s)(\hat{\gamma}_s - \lambda_s)\dot{\hat{\gamma}}_s \end{aligned} \tag{18}$$

where $\dot{\tilde{\boldsymbol{\delta}}}_{\mathbf{x},i} = \dot{\hat{\boldsymbol{\delta}}}_{\mathbf{x},i}$ because $\tilde{\boldsymbol{\delta}}_{\mathbf{x},i} = \hat{\boldsymbol{\delta}}_{\mathbf{x},i} - \boldsymbol{\delta}_{\mathbf{x},i}$ and the actual system's parameters are constant: $\boldsymbol{\delta}_{\mathbf{x},i} = 0$. Using $\mathbf{M}_{\mathbf{x},m}\dot{\boldsymbol{\varepsilon}}_m$ and $\mathbf{M}_{\mathbf{x},s}\dot{\boldsymbol{\varepsilon}}_s$ from (15) and (16), and based on Property 2 of the robot dynamics ($\dot{\mathbf{M}}_{\mathbf{x},i} - 2\mathbf{C}_{\mathbf{x},i}$ is skew symmetric), Eq. (18) is found as

$$\begin{aligned} \dot{V}(t) = &\boldsymbol{\varepsilon}_m^T\mathbf{R}_{\mathbf{x},m}\tilde{\boldsymbol{\delta}}_{\mathbf{x},m} + \dot{\hat{\boldsymbol{\delta}}}_{\mathbf{x},m}^T\boldsymbol{\Psi}_m^{-1}\tilde{\boldsymbol{\delta}}_{\mathbf{x},m} \\ &+ \boldsymbol{\varepsilon}_m^T(\mathbf{u}_{\mathbf{x},m} - \hat{\gamma}_m\,\mathrm{sgn}(\boldsymbol{\varepsilon}_m)) + (1/\rho_m)(\hat{\gamma}_m - \lambda_m)\dot{\hat{\gamma}}_m \\ &- \beta_{3,m}\boldsymbol{\varepsilon}_m^T\mathbf{M}_{\mathbf{x},m}\boldsymbol{\varepsilon}_m \\ &+ \boldsymbol{\varepsilon}_s^T\mathbf{R}_{\mathbf{x},s}\tilde{\boldsymbol{\delta}}_{\mathbf{x},s} + \dot{\hat{\boldsymbol{\delta}}}_{\mathbf{x},s}^T\boldsymbol{\Psi}_s^{-1}\tilde{\boldsymbol{\delta}}_{\mathbf{x},s} \\ &+ \boldsymbol{\varepsilon}_s^T(\mathbf{u}_{\mathbf{x},s} - \hat{\gamma}_s\,\mathrm{sgn}(\boldsymbol{\varepsilon}_s)) + (1/\rho_s)(\hat{\gamma}_s - \lambda_s)\dot{\hat{\gamma}}_s \\ &- \beta_{3,s}\boldsymbol{\varepsilon}_s^T\mathbf{M}_{\mathbf{x},s}\boldsymbol{\varepsilon}_s \end{aligned} \tag{19}$$

### 5.2. First Adaptation Law (for Uncertain Dynamic Parameters)

The first adaptation law for updating the estimated parameters of the robotic tele-rehabilitation system is presented for the master and slave as

$$\dot{\hat{\boldsymbol{\delta}}}_{\mathbf{x},m} = -\boldsymbol{\Psi}_m^T\mathbf{R}_{\mathbf{x},m}^T\boldsymbol{\varepsilon}_m\ , \quad \dot{\hat{\boldsymbol{\delta}}}_{\mathbf{x},s} = -\boldsymbol{\Psi}_s^T\mathbf{R}_{\mathbf{x},s}^T\boldsymbol{\varepsilon}_s \tag{20}$$

such that the terms including $\tilde{\boldsymbol{\delta}}_{\mathbf{x},m}$ and $\tilde{\boldsymbol{\delta}}_{\mathbf{x},s}$ in (19) are cancelled, i.e., the bilateral adaptive controller becomes robust against the parametric uncertainties. Having $\boldsymbol{\varepsilon}_i^T \operatorname{sgn}(\boldsymbol{\varepsilon}_i) = \|\boldsymbol{\varepsilon}_i\|_1$ and using the adaptation law (20) for the system parameters in (19), the Lyapunov function's time derivative is obtained as

$$\begin{aligned}\dot{V}(t) = {} & \boldsymbol{\varepsilon}_m^T \mathbf{u}_{\mathbf{x},m} - \hat{\gamma}_m \|\boldsymbol{\varepsilon}_m\|_1 + (1/\rho_m)(\hat{\gamma}_m - \lambda_m)\dot{\hat{\gamma}}_m \\ & - \beta_{3,m} \boldsymbol{\varepsilon}_m^T \mathbf{M}_{\mathbf{x},m} \boldsymbol{\varepsilon}_m \\ & + \boldsymbol{\varepsilon}_s^T \mathbf{u}_{\mathbf{x},s} - \hat{\gamma}_s \|\boldsymbol{\varepsilon}_s\|_1 + (1/\rho_s)(\hat{\gamma}_s - \lambda_s)\dot{\hat{\gamma}}_s \\ & - \beta_{3,s} \boldsymbol{\varepsilon}_s^T \mathbf{M}_{\mathbf{x},s} \boldsymbol{\varepsilon}_s\end{aligned} \tag{21}$$

### 5.3. Second Adaptation Law (for Varying Robust Gains)

The second adaptation law for updating the robust gains $\hat{\gamma}_m$ and $\hat{\gamma}_s$ of the bilateral controller (9) and (10) is introduced as

$$\begin{aligned}\dot{\hat{\gamma}}_m &= \rho_m \|\boldsymbol{\varepsilon}_m\|_1 , \quad \hat{\gamma}_m(0) = \hat{\gamma}_{m0} > 0 \\ \dot{\hat{\gamma}}_s &= \rho_s \|\boldsymbol{\varepsilon}_s\|_1 , \quad \hat{\gamma}_s(0) = \hat{\gamma}_{s0} > 0\end{aligned} \tag{22}$$

where $\hat{\gamma}_{m0}$ and $\hat{\gamma}_{s0}$ are the positive initial values of the robust gains (at $t = 0$). Employing the above-mentioned adaptation law (22) in (21), $\dot{V}(t)$ is simplified as

$$\begin{aligned}\dot{V}(t) = {} & \boldsymbol{\varepsilon}_m^T \mathbf{u}_{\mathbf{x},m} - \lambda_m \|\boldsymbol{\varepsilon}_m\|_1 - \beta_{3,m} \boldsymbol{\varepsilon}_m^T \mathbf{M}_{\mathbf{x},m} \boldsymbol{\varepsilon}_m \\ & + \boldsymbol{\varepsilon}_s^T \mathbf{u}_{\mathbf{x},s} - \lambda_s \|\boldsymbol{\varepsilon}_s\|_1 - \beta_{3,s} \boldsymbol{\varepsilon}_s^T \mathbf{M}_{\mathbf{x},s} \boldsymbol{\varepsilon}_s\end{aligned} \tag{23}$$

According to the boundedness of the unstructured (non-parametric) uncertainties $\mathbf{u}_{\mathbf{x},m}$ and $\mathbf{u}_{\mathbf{x},s}$ expressed in (5), the Lyapunov function's time derivative is finally obtained as

$$\dot{V}(t) \le -\beta_{3,m} \boldsymbol{\varepsilon}_m^T \mathbf{M}_{\mathbf{x},m} \boldsymbol{\varepsilon}_m - \beta_{3,s} \boldsymbol{\varepsilon}_s^T \mathbf{M}_{\mathbf{x},s} \boldsymbol{\varepsilon}_s \tag{24}$$

Thus, the robust gains $\hat{\gamma}_m$ and $\hat{\gamma}_s$ of the controller are updated based on (22) such that the controlled system becomes robust against bounded unstructured uncertainties $\mathbf{u}_{\mathbf{x},m}$ and $\mathbf{u}_{\mathbf{x},s}$ without any information about their upper bounds $\lambda_m$ and $\lambda_s$ introduced in (5).

### 5.4. Tracking Convergence Proof

**Theorem.** Assuming the Lyapunov function (17) is positive definite ($V(t) > 0$) and its time derivative (24) is negative semi-definite ($\dot{V}(t) \le 0$) in terms of the uniformly positive definite matrices $\mathbf{M}_{\mathbf{x},m}$, $\mathbf{M}_{\mathbf{x},s}$, $\boldsymbol{\Psi}_m$ and $\boldsymbol{\Psi}_s$, the tracking convergence of the master and slave trajectories to their desired responses ($\mathbf{x}_m \to \mathbf{x}_{des_m}$ and $\mathbf{x}_s \to \mathbf{x}_{des_s}$) and the boundedness of $\tilde{\boldsymbol{\delta}}_{\mathbf{x},m}$, $\tilde{\boldsymbol{\delta}}_{\mathbf{x},s}$, $(\hat{\gamma}_m - \lambda_m)$ and $(\hat{\gamma}_s - \lambda_s)$ are guaranteed.

**Proof.** If $g$ is a uniformly continuous function for $t \ge 0$ and $\lim_{t\to\infty} \int_0^t g(\phi)\, d\phi$ has a finite value; then, it is concluded based on the Barbalat's lemma [51] that: $\lim_{t\to\infty} g(t) = 0$.

Now, $g(t) = \beta_{3,m} \boldsymbol{\varepsilon}_m^T \mathbf{M}_{\mathbf{x},m} \boldsymbol{\varepsilon}_m + \beta_{3,s} \boldsymbol{\varepsilon}_s^T \mathbf{M}_{\mathbf{x},s} \boldsymbol{\varepsilon}_s \ge 0$ is considered as a uniformly continuous function. To elaborate more on that, the time derivative of this function is obtained as $\dot{g}(t) = 2\beta_{3,m} \boldsymbol{\varepsilon}_m^T \mathbf{M}_{\mathbf{x},m} \dot{\boldsymbol{\varepsilon}}_m + 2\beta_{3,s} \boldsymbol{\varepsilon}_s^T \mathbf{M}_{\mathbf{x},s} \dot{\boldsymbol{\varepsilon}}_s + \beta_{3,m} \boldsymbol{\varepsilon}_m^T \dot{\mathbf{M}}_{\mathbf{x},m} \boldsymbol{\varepsilon}_m + \beta_{3,s} \boldsymbol{\varepsilon}_s^T \dot{\mathbf{M}}_{\mathbf{x},s} \boldsymbol{\varepsilon}_s$. Since the Lyapunov function is bounded as $V(t) \ge 0$ and $\dot{V}(t) \le 0$, and due to (17), $\boldsymbol{\varepsilon}_m$, $\boldsymbol{\varepsilon}_s$, $\tilde{\boldsymbol{\delta}}_{\mathbf{x},m}$, $\tilde{\boldsymbol{\delta}}_{\mathbf{x},s}$, $(\hat{\gamma}_m - \lambda_m)$ and $(\hat{\gamma}_s - \lambda_s)$ are all bounded. Based on the closed-loop dynamics (15) and (16) of the master and slave robots, the system responses ($\dot{\boldsymbol{\varepsilon}}_m$ and $\dot{\boldsymbol{\varepsilon}}_s$) to the bounded motor inputs and disturbances remain bounded. Moreover, the elements of the non-singular inertia matrices $\mathbf{M}_{\mathbf{x},m}$ and $\mathbf{M}_{\mathbf{x},s}$ are bounded and differentiable in terms of robots' positions, and their time derivatives $\dot{\mathbf{M}}_{\mathbf{x},m}$ and $\dot{\mathbf{M}}_{\mathbf{x},s}$ are bounded in terms of robots' positions and velocities. Consequently, $\dot{g}(t)$ is bounded and $g(t)$ is uniformly continuous. Then, it can be written by integrating Eq. (24) over the time that:

$$V(0) - V(\infty) \ge \lim_{t\to\infty} \int_0^t g(\varphi)\, d\phi \tag{25}$$

Also, since $\dot{V}(t) = dV(t)/dt \le 0$ is negative based on Eq. (24), $V(0) - V(\infty) \ge 0$ is positive and finite. Therefore, $\lim_{t\to\infty} \int_0^t g(\phi)\, d\phi$

in (25) exists and has a finite and positive value from the positiveness of $g(t)$. As a result, it is obtained according to the Barbalat's lemma [51] that:

$$\lim_{t\to\infty} g(t) = \lim_{t\to\infty} \left( \beta_{3,m} \boldsymbol{\varepsilon}_m^T \mathbf{M}_{\mathbf{x},m} \boldsymbol{\varepsilon}_m + \beta_{3,s} \boldsymbol{\varepsilon}_s^T \mathbf{M}_{\mathbf{x},s} \boldsymbol{\varepsilon}_s \right) = 0 \qquad (26)$$

Since $\beta_{3,m} > 0$ and $\beta_{3,s} > 0$ are nonzero positive constants, and $\boldsymbol{\varepsilon}_m^T \mathbf{M}_{\mathbf{x},m} \boldsymbol{\varepsilon}_m \geq 0$ and $\boldsymbol{\varepsilon}_s^T \mathbf{M}_{\mathbf{x},s} \boldsymbol{\varepsilon}_s \geq 0$, Eq. (26) guarantees the convergence to sliding surfaces $\boldsymbol{\varepsilon}_m = 0$ and $\boldsymbol{\varepsilon}_s = 0$ as $t \to \infty$. Based on the convergence of $\boldsymbol{\varepsilon}_m \to 0$ and $\boldsymbol{\varepsilon}_s \to 0$ and the boundedness of $V(t)$, it is concluded from Eq. (17) that the errors of parameter estimation $\tilde{\boldsymbol{\delta}}_{\mathbf{x},m}$ and $\tilde{\boldsymbol{\delta}}_{\mathbf{x},s}$ and also the differences between the updated robust gains and the bounds of unstructured uncertainties $(\hat{\gamma}_m - \lambda_m)$ and $(\hat{\gamma}_s - \lambda_s)$ all remain bounded.

Finally, based on the stable dynamics of the master's and slave's sliding surfaces $\boldsymbol{\varepsilon}_m$ and $\boldsymbol{\varepsilon}_s$ in (7), the convergence of tracking errors to zero $\tilde{\mathbf{x}}_m \to 0$ and $\tilde{\mathbf{x}}_s \to 0$ are established on the surfaces of $\boldsymbol{\varepsilon}_m = 0$ and $\boldsymbol{\varepsilon}_s = 0$. Therefore, the proposed nonlinear bilateral robust adaptive controller ensures that the master and slave robots track their corresponding desired trajectories: $\mathbf{x}_m \to \mathbf{x}_{des_m}$ and $\mathbf{x}_s \to \mathbf{x}_{des_s}$ during physical interaction with the patient and therapist, respectively. ■

### 5.5. Safety in the Robotic Tele-rehabilitation System

As mentioned in Sec. 2.6, the stability of the desired impedance model (2) with positive parameters implies that the bounded forces of the patient $\mathbf{f}_{pa}$ and therapist $\mathbf{f}_{th}$ will produce bounded desired trajectories for the master ($\mathbf{x}_{des_m}$) and slave ($\mathbf{x}_{des_s}$) robots. In addition, the presented Lyapunov stability proof guarantees the boundedness of the tracking errors ($\boldsymbol{\varepsilon}_m$ and $\boldsymbol{\varepsilon}_s$) and their convergence to zero ($\boldsymbol{\varepsilon}_m \to 0$ and $\boldsymbol{\varepsilon}_s \to 0$ that results $\mathbf{x}_m \to \mathbf{x}_{des_m}$ and $\mathbf{x}_s \to \mathbf{x}_{des_s}$) using the proposed nonlinear bilateral robust adaptive controller. Moreover, the stability and tracking convergence characteristics are proven in the presence of parametric and non-parametric uncertainties that commonly exist in the experimental setups. Based on the combination of the desired impedance model's stability and the Lyapunov stability of the closed-loop nonlinear dynamics of the telerobotic system, the bounded interaction forces of the patient ($\mathbf{f}_{pa}$) and the therapist ($\mathbf{f}_{th}$) will make bounded responses in master ($\mathbf{x}_m$) and slave ($\mathbf{x}_s$) trajectories and do not destabilize the robots. The stability feature of the proposed strategy enhances the safety of the patient and therapist during the task, which is an important concern in robotic tele-rehabilitation systems [14].

## 6. Experiments

The functionality of the proposed impedance-controlled tele-rehabilitation strategy was evaluated experimentally using a 2-DOF planar Quanser Rehab Robot (Quanser Consulting Inc., Markham, Canada) designed for the upper limb as the master, and a 3-DOF Phantom Premium 1.5A robot (Geomagic Inc., Wilmington, USA) employed as the slave (Fig. 5). The Phantom Premium and Quanser Rehab robots were equipped with an ATI Nano43 and an ATI Gamma force/torque sensors (ATI Industrial Automation, Apex, USA), respectively, to measure the therapist's and the patient's interaction forces. The QUARC (Quanser Real-Time Control) environment was used as the control software to implement the proposed bilateral robust adaptive controller with 1 $m$sec sampling time.

As the first step towards the experimental evaluation of the proposed control concept, the following tests involved a healthy human operator as the therapist. Several different features and adjustments of the proposed strategy for tele-rehabilitation were tested.

### 6.1. A Resistive Stiff Environment as a Disabled Patient

As shown in Fig. 5, the proposed assistive tele-rehabilitation strategy was first evaluated using a stiff environment designed to generate a pre-specified resistive centripetal interaction force on the master robot (as the patient's force). With this configuration, the performance of the impedance-based

controller is analyzed more systematically than when a human with physical impairments is involved. The interaction with a resistive environment is similar to an interaction with a patient who has low capability of movement generation from his rest configuration. In these cases, the patient has a fixed arm position that is naturally hard for him to move from this stationary configuration due to his disabilities. For such a person, his interaction force with the robot is toward this natural equilibrium position similar to the set of springs in Fig. 5. In this case, the patient/master trajectory has a deviation with respect to the target during the entire path.

It is notable that the provided stiff environment can not exactly simulate the physical interaction of a patient with weakened muscle activity and other motor control problems. For example, the hand tremor (that generates high-frequency interaction forces) cannot be provided using such environments. Thus, more realistic patient behavior, including hand tremor, is tried to be simulated by an able-bodied human operator in the next part of experiments (Sec. 6.2).

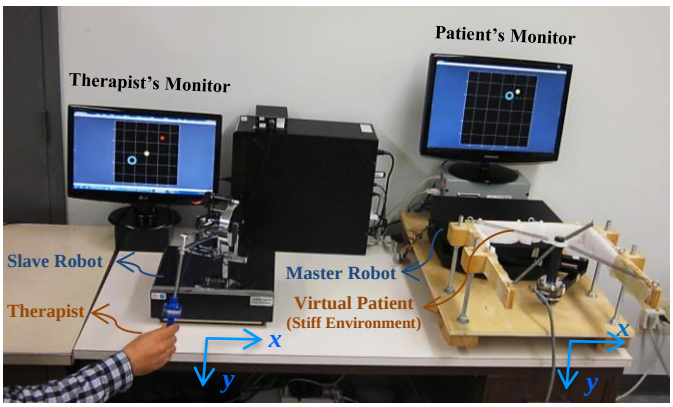


Fig. 5. The telerobotic experimental set-up for the first evaluations of assistive tele-rehabilitation strategy: the Quanser Rehab robot (right) is the master, the Phantom Premium robot (left) is the slave, and the patient force is modeled with the centripetal force of the stiff environment.

The therapist had a computer monitor to observe the patient/ master's deviation from the target in the $x-y$ plane shown by the hollow blue circle; this deviation was tracked by the slave robot and thus felt by the therapist's hand. The center of the therapist's monitor was shown by a solid yellow circle. The position difference of these blue and yellow circles visually informed the therapist about the magnitude and direction of the patient's deviation and helped the therapist to apply the desired force to decrease this deviation. Accordingly, if the therapist wanted to bring the patient's limb back on the moving target, he had to bring the blue circle on the yellow one (at the origin). The position of the moving target was also shown by a red circle such that the therapist knew about the target in addition to the patient's deviation. On the other side, the patient's monitor showed the positions of the master robot (or the patient's limb) and the moving target on the $x-y$ plane as the hollow blue and solid yellow circles, respectively. If the patient decreased his deviation with the therapist's assistance in order to move with the target, the blue circle was on the yellow one in a way similar to the therapist's screen.

Note that the workspace of the master (Quanser Rehab) robot is in the horizontal $x-y$ space as shown in Fig. 5. Also, the slave (Phantom Premium) robot was controlled such that its end-effector had motions in the same two-dimensional $x-y$ coordinates. Therefore, the Cartesian position of master and robots' end-effector is expressed as $\mathbf{x}_i=[x \quad y]_i^T$ (where $i=m$ and $s$). The kinematics and dynamics of the Quanser Rehab (master) and Phantom Premium (slave) robots were comprehensively presented and described in [54, 55] and [56], respectively.

The parameters of the desired impedance model (2) were chosen for three different levels of assistance during the tracking of the moving target, as summarized in Table 1. In these experiments, the stiffness parameter $k_{des}$ of the impedance model (2) was designed first based on the desired relationship between the forces ($\mathbf{f}_{pa}$, $\mathbf{f}_{th}$) and the position deviation $(\mathbf{x}_{des_m}-\mathbf{x}_{tar})$. As the stiffness value decreases, the patient's position deviation increases in response to the specified values of the interaction forces, i.e., the patient's limb is less forcefully attracted to the target's position. Therefore, the level of assistance during the process of movement therapy decreases by the decrease of the stiffness parameter $k_{des}$, which can be adjusted by the therapist in response to the patient's improvement during the tele-rehabilitation process. The

damping ratio of the impedance model (2) as a second-order differential equation was adjusted as $\zeta = c_{des}/2\sqrt{m_{des}k_{des}} = 0.7$ such that the impedance model had an underdamped response with respect to the dimensionless time $\omega_n t$ (also with appropriate overshoot value in response to the step forces). The natural frequency of desired impedance model (2) was adjusted on $\omega_n = \sqrt{k_{des}/m_{des}} = 15$ rad/sec in order to have a fast response to the therapist's and patient's forces. Moreover, the force scaling factor was chosen $\alpha_{\mathrm{f}} = 4$ such that the therapist had four times more authority in comparison with the patient. Accordingly, the therapist could easily manipulate the patient's deviation $(\mathbf{x}_{des_m} - \mathbf{x}_{tar})$ as the response of Eq. (2) by applying a small force $\mathbf{f}_{th}$ during the tele-rehabilitation. The position scaling factor was also considered to be $\alpha_{\mathrm{x}} = 3$ to amplify the patient deviation from the target's trajectory and then provide it for the therapist's hand using the slave robot. The impedance parameters and scaling factors employed in the first part of the experiments are summarized in Table 1. Three different values of the stiffness parameter $k_{des}$ were considered for three levels of assistance without regarding to the therapist's assistive force. Then, using $\omega_n = \sqrt{k_{des}/m_{des}} = 15$ rad/sec and $\zeta = c_{des}/2\sqrt{m_{des}k_{des}} = 0.7$, the values of damping $c_{des}$ and mass $m_{des}$ parameters were determined for each level.

The parameters of the proposed nonlinear bilateral control laws (9) and (10) and two adaptation laws (20) and (22) used in the experiments are listed in Table 2. These parameters are obtained using a trial-and-error method and performing some initial experiments. This adjustment resulted in acquiring an optimum stability performance of the teleoperation system and achieving an appropriate tracking convergence to the desired responses for the master and slave robots (with suitable transient behaviors and enough small steady-state errors). For instance, the initial values of the robust gains $\hat{\gamma}_{m0}$ and $\hat{\gamma}_{s0}$ in (22) are specified to overcome the minimum level of possible disturbances $\mathbf{u}_{\mathbf{x},m}$ and $\mathbf{u}_{\mathbf{x},s}$. Their update rates $\rho_m$ and $\rho_s$ are also regulated to be large enough in order to increase the time-varying robust gains $\hat{\gamma}_m$ and $\hat{\gamma}_s$ fast enough to overcome unknown disturbances and their variations during the task, which leads to maintaining small tracking errors $\boldsymbol{\varepsilon}_m$ and $\boldsymbol{\varepsilon}_s$.

Table 1. The impedance parameters and scaling factors for three levels of assistance

| Level of Assistance | Desired Impedance Model Parameters | Scaling Factors |
|---|---|---|
| Level 1 (high assistance) | $k_{des} = 400$ N/m<br>$c_{des} = 37.33$ N.s/m<br>$m_{des} = 1.78$ kg | $\alpha_{\mathrm{f}} = 4$<br>$\alpha_{\mathrm{x}} = 3$ |
| Level 2 (medium assistance) | $k_{des} = 200$ N/m<br>$c_{des} = 18.66$ N.s/m<br>$m_{des} = 0.89$ kg | $\alpha_{\mathrm{f}} = 4$<br>$\alpha_{\mathrm{x}} = 3$ |
| Level 3 (low assistance) | $k_{des} = 100$ N/m<br>$c_{des} = 9.33$ N.s/m<br>$m_{des} = 0.45$ kg | $\alpha_{\mathrm{f}} = 4$<br>$\alpha_{\mathrm{x}} = 3$ |

Note that functions $\mathrm{sgn}(\boldsymbol{\varepsilon}_m)$ and $\mathrm{sgn}(\boldsymbol{\varepsilon}_s)$ in the master and slave control laws (9) and (10) were replaced by continuous functions $\tanh(150\boldsymbol{\varepsilon}_m)$ and $\tanh(150\boldsymbol{\varepsilon}_s)$, respectively, in order to prevent undesired discontinuities and chattering in the input torques.

In these experimental evaluations of the proposed tele-rehabilitation strategy, the moving target was considered to have an absolute velocity of $V_{tar} = 0.05$ m/sec in a circular path in the $x-y$ plane with the radius of $r_{tar} = 0.1$ m. Note that circular trajectories are usually employed in therapeutic exercises and especially robotic rehabilitation.

Table 2. Employed parameter values in the bilateral control laws and two adaptation laws

| Parameters of Control Laws | Parameters of Adaptation Laws |
|---|---|
| $\beta_{1,m} = 1.6$, $\beta_{1,s} = 1.6$ | $\boldsymbol{\Psi}_m = 42I$, $\boldsymbol{\Psi}_s = 15I$ |
| $\beta_{2,m} = 0.64$, $\beta_{2,s} = 0.64$ | $\rho_m = 1.6$, $\hat{\gamma}_{m0} = 0.25$ |
| $\beta_{3,m} = 240$, $\beta_{3,s} = 70$ | $\rho_s = 1.2$, $\hat{\gamma}_{s0} = 0.12$ |

### *6.1.1. Cartesian to Cartesian Mapping*

The performance of the proposed strategy in tracking the moving target with a Cartesian to Cartesian mapping was illustrated visually on the therapist and patient monitors, as shown in Fig. 6. The scaled patient's deviation from the target in the Cartesian space is seen in the therapist's monitor in the same Cartesian space (Fig. 6a), and the patient's Cartesian position with respect to the moving target is observed on the patient's monitor (Fig. 6b).

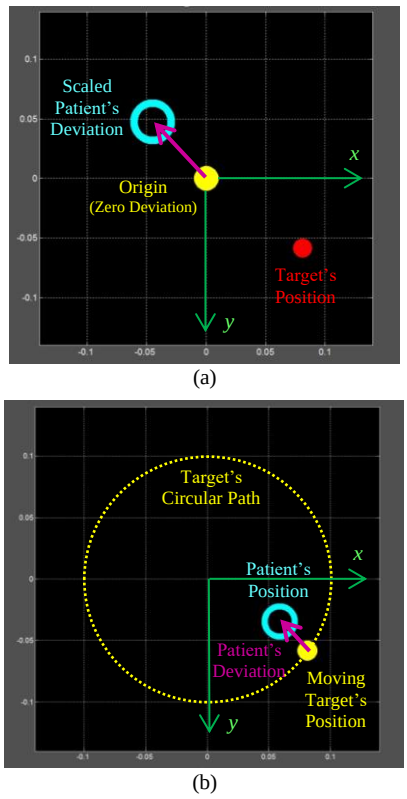


Fig. 6. The position data illustrated for Cartesian to Cartesian mapping on (a) the therapist's and (b) the patient's monitors for tracking the moving target via the proposed assist-as-needed tele-rehabilitation strategy (some notes about the patient and moving target positions and the patient's deviation are added).

The position of the master robot's end-effector $\mathbf{x}_m$ (patient) in tracking its desired trajectory $\mathbf{x}_{des_m}$ together with the target's position $\mathbf{x}_{tar}$ in $x$ and $y$ Cartesian coordinates for Level 1 of assistance (see Table 1) are shown in Fig. 7. As seen, before the therapist's intervention, the virtual patient (stiff environment) has a small deviation from the target's position toward the origin as the natural equilibrium position of the springs (Fig. 5). However, after that the therapist applies an assistive force to decrease the patient's deviation $(\mathbf{x}_m - \mathbf{x}_{tar}) \to 0$, the target's trajectory is tracked well by the patient. Figure 8 shows the position of the slave robot's end-effector $\mathbf{x}_s$ (therapist) in tracking the scaled master/patient position deviation with respect to the target $\alpha_x(\mathbf{x}_m - \mathbf{x}_{tar})$ as the slave desired trajectory $\mathbf{x}_{des_s}$. As seen, the therapist tries to decrease the scaled patient-target deviation (sensed by the slave robot and seen in his monitor) to zero by applying the force $\mathbf{f}_{th}$ after $t = 50.2$ sec (see Fig. 9).

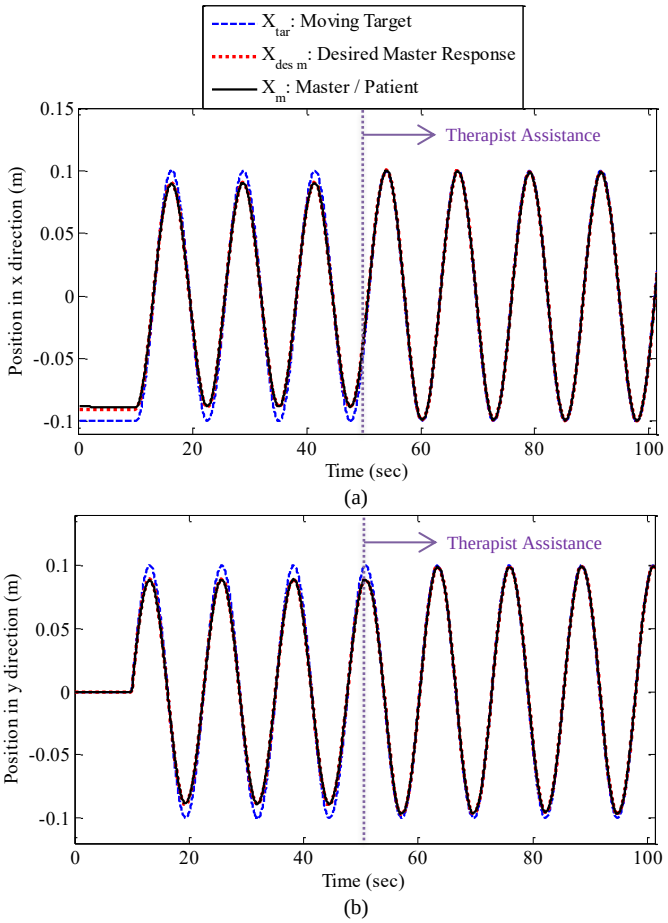


Fig. 7. The target's position $\mathbf{x}_{tar}$ together with the desired and actual positions of the master robot's end-effector/patient ($\mathbf{x}_{des_m}$, $\mathbf{x}_m$), in (a) $x$ and (b) $y$ directions of Cartesian coordinates for the Level 1 of assistance (see Table 1).

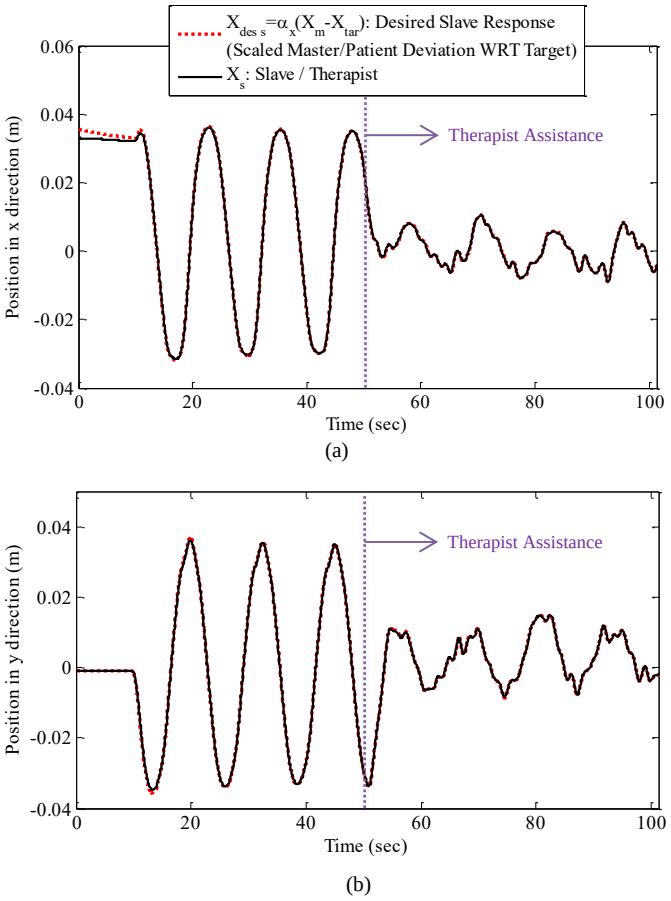


Fig. 8. Position of the slave robot's end-effector $\mathbf{x}_s$ (therapist) in tracking its desired trajectory $\mathbf{x}_{des_s}$ that is the scaled master/patient position deviation with respect to the target $\alpha_x(\mathbf{x}_m - \mathbf{x}_{tar})$ with $\alpha_x = 3$, in (a) $x$ and (b) $y$ directions of Cartesian coordinates for the Level 1 of assistance (see Table 1).

As shown in Fig. 9, the patient's resistive force $\mathbf{f}_{pa}$ (before the therapist assistance) has an approximate maximum magnitude of 4.4 N in the $x$ direction. This force generates an approximate maximum deviation of 0.011 m in the $x$ direction (seen in Fig. 7) between the patient and target positions based on Eq. (2) and due to the employed impedance parameters (including $k_{des} = 400$ N/m) for the high level of assistance (Level 1 in Table 1). Also, the slave robot, which tracks the scaled-up version of the patient-target deviation using $\alpha_x = 3$, has the approximate motion magnitude of $3 \times 0.011 = 0.033$ m in the $x$ direction (observed in Fig. 8a) before applying the therapist's interaction force. However, after $t = 50.2$ sec when the therapist attempts to bring the patient's position to the target ($\mathbf{x}_m \rightarrow \mathbf{x}_{tar}$), the scaled version of his assistive force (see Fig. 9) neutralizes the patient's force $(\mathbf{f}_{pa} - \alpha_f \mathbf{f}_{th}) \rightarrow 0$. This force tracking being coincident with the target tracking is in accordance with the presented discussion in Sec. 2.2. Note that the patient's force increases after the therapist's assistance for the target tracking in comparison with the one before the therapist's intervention. This is because the stiff environment (behaving as the virtual patient) is extended much farther from its equilibrium position (at the center) when the master robot exactly tracks the target's trajectory without any deviation (toward the center).

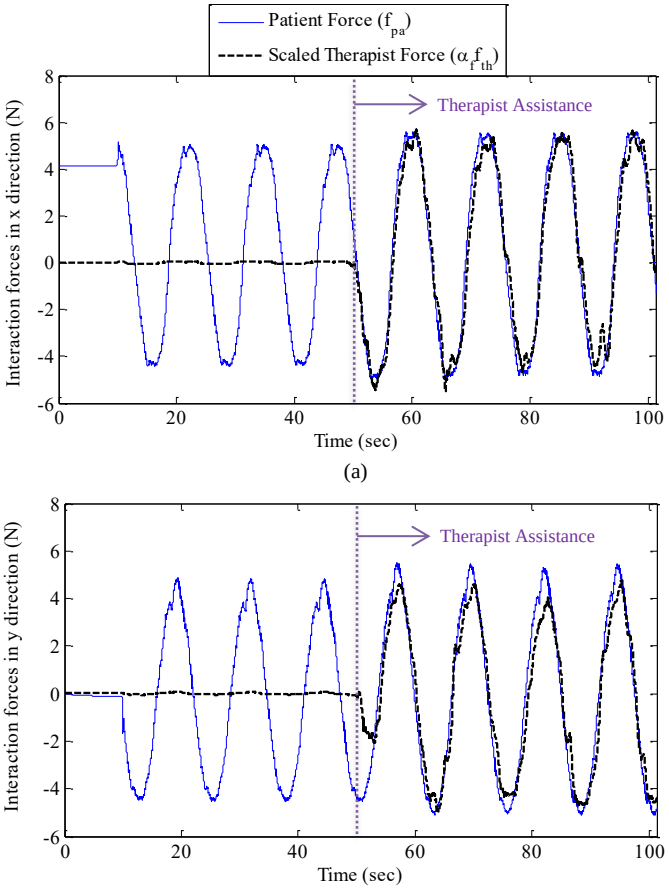


Fig. 9. The patient's force $\mathbf{f}_{pa}$ and the scaled therapist force $\alpha_f \mathbf{f}_{th}$ in (a) $x$ and (b) $y$ directions: the assistive force of the therapist starts at $t = 50.2$ sec and the force reflection $(\mathbf{f}_{pa} - \alpha_f \mathbf{f}_{th}) \rightarrow 0$ is obtained after this time.

To elaborate on the performance of the proposed nonlinear bilateral controller, the position tracking errors of the master ($\tilde{\mathbf{x}}_m = \mathbf{x}_m - \mathbf{x}_{des_m}$) and slave ($\tilde{\mathbf{x}}_s = \mathbf{x}_s - \mathbf{x}_{des_s}$) are shown in Fig.

10. As seen, the tracking errors converge to zero ($\tilde{\mathbf{x}}_m \to 0$ and $\tilde{\mathbf{x}}_s \to 0$) using the proposed control laws, which is in accordance with the convergence and stability proof presented in Sec. 5.

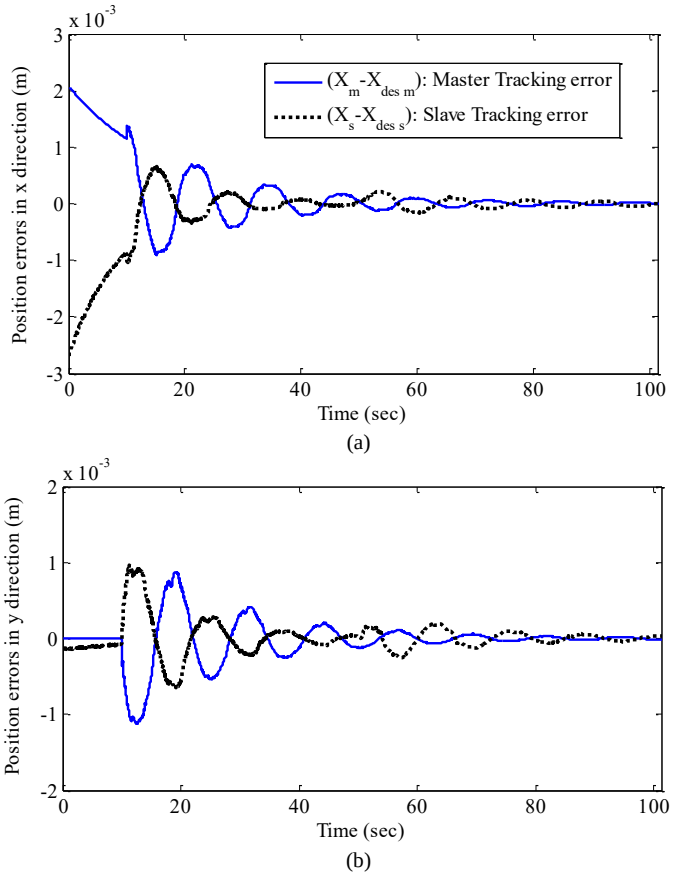


Fig. 10. The convergence of the master ($\tilde{\mathbf{x}}_m = \mathbf{x}_m - \mathbf{x}_{des_m}$) and slave ($\tilde{\mathbf{x}}_s = \mathbf{x}_s - \mathbf{x}_{des_s}$) tracking errors to zero using the proposed control strategy, (a) in $x$ and (b) in $y$ directions, for the Level 1 of assistance (Table 1).

Now, the results of Level 2 of assistance (parameterized in Table 1) using the stiff environment as the virtual patients are reported. The positions of the master robot's end-effector $\mathbf{x}_m$ (patient), its desired trajectory $\mathbf{x}_{des_m}$, and the target $\mathbf{x}_{tar}$ in $x$ direction are shown in Fig. 11a. As observed, before the therapist assistance, the virtual patient (stiff environment) has approximately two times larger deviation (about 0.022 m in $x$ direction) from the target's position in comparison with Level 1 (shown in Fig. 7). The positions of the slave robot's end-effector $\mathbf{x}_s$ (therapist) and its desired trajectory $\mathbf{x}_{des_s}$ (the scaled master/patient position deviation with respect to the target) are illustrated in Fig. 11b, which shows approximately two times larger patient-target deviation in comparison with Level 1 of assistance (Fig. 8). This increased deviation in Level 2 of assistance is due to the decrease of impedance parameters to half of ones used in Level 1 (see Table 1), and the similar patient force generated by the stiff environment (see Figs. 9a and 11c). As seen, the therapist tries to decrease the scaled patient-target deviation to zero after $t = 48.1$ sec by adjusting his force $\mathbf{f}_{th}$ shown in Fig. 11c.

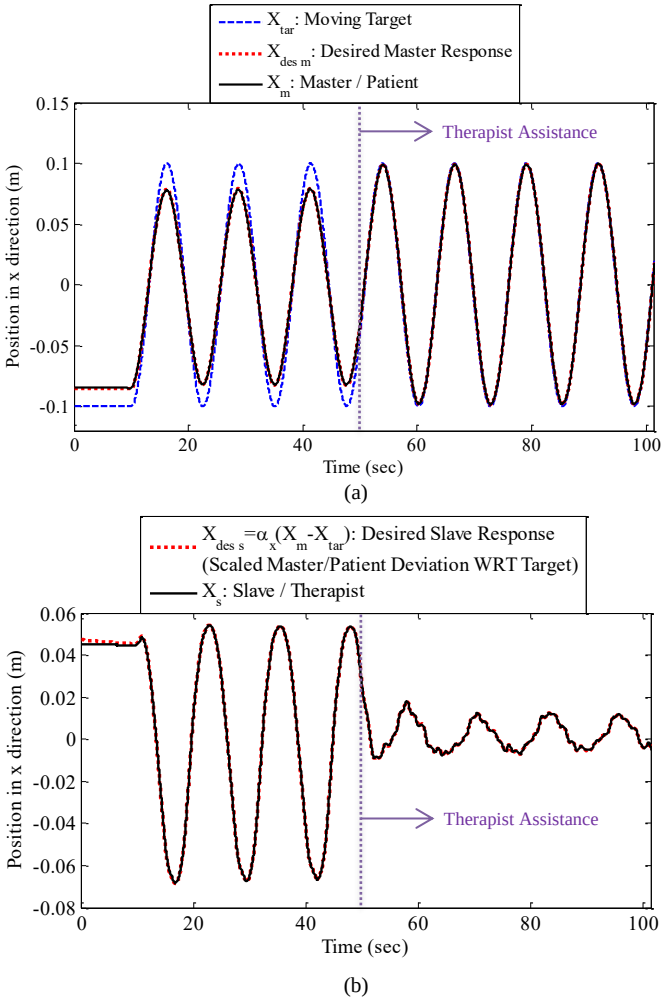

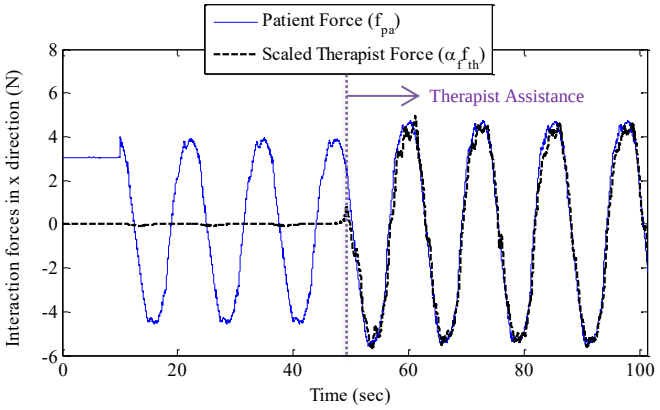


(c)

Fig. 11. (a) The target's position $\mathbf{x}_{tar}$ and the positions of the master robot's end-effector $\mathbf{x}_m$ (patient) and its desired response $\mathbf{x}_{des_m}$, (b) the positions of the slave robot's end-effector $\mathbf{x}_s$ (therapist) and its desired response $\mathbf{x}_{des_s}$ (the scaled master/patient position deviation with respect to the target $\alpha_x(\mathbf{x}_m - \mathbf{x}_{tar})$ with $\alpha_x = 3$), and (c) the patient's force $\mathbf{f}_{pa}$ and the scaled therapist force $\alpha_f \mathbf{f}_{th}$ (where the assistive force of therapist starts from $t = 48.1$ sec), all in $x$ direction for the Level 2 of assistance (in Table 1).

Finally, the desired and actual positions of the master ($\mathbf{x}_{des_m}$, $\mathbf{x}_m$) and the slave ($\mathbf{x}_{des_s}$, $\mathbf{x}_s$) are shown in Fig. 12a and 12b, respectively, for Level 3 of assistance (introduced in Table 1). Since the impedance parameters in Level 3 were smaller than the ones in Levels 2 and 1, the patient's deviation from the target's position (shown in Fig. 12a) is approximately two and four times larger in comparison with the deviations in Level 2 (Fig. 11a) and Level 1 (Fig. 7a), respectively. The patient's force field was the same as the previous cases employing the same stiff environment as the virtual patient. However, the magnitude of the patient's force (Fig. 12c) before the therapist's assistance was less than the previous cases (Figs. 9a and 11c) due to the much higher deviation of the springs (stiff environment) toward their equilibrium position at the center in comparison with the previous cases. This causes that the magnitude of the patient-target deviation in Level 3 (Fig. 12b) is not exactly two and four times larger than the ones obtained in Level 2 (Fig. 11b) and Level 1 (Fig. 8a). The same behavior is seen by comparing the force magnitudes between Level 2 (Fig. 11c) and Level 1 (Fig. 9a). Similar to previous cases, the therapist applied his interaction force $\mathbf{f}_{th}$ after $t = 53.4$ sec (as demonstrated in Fig. 12c) in order to decrease the patient's deviation.

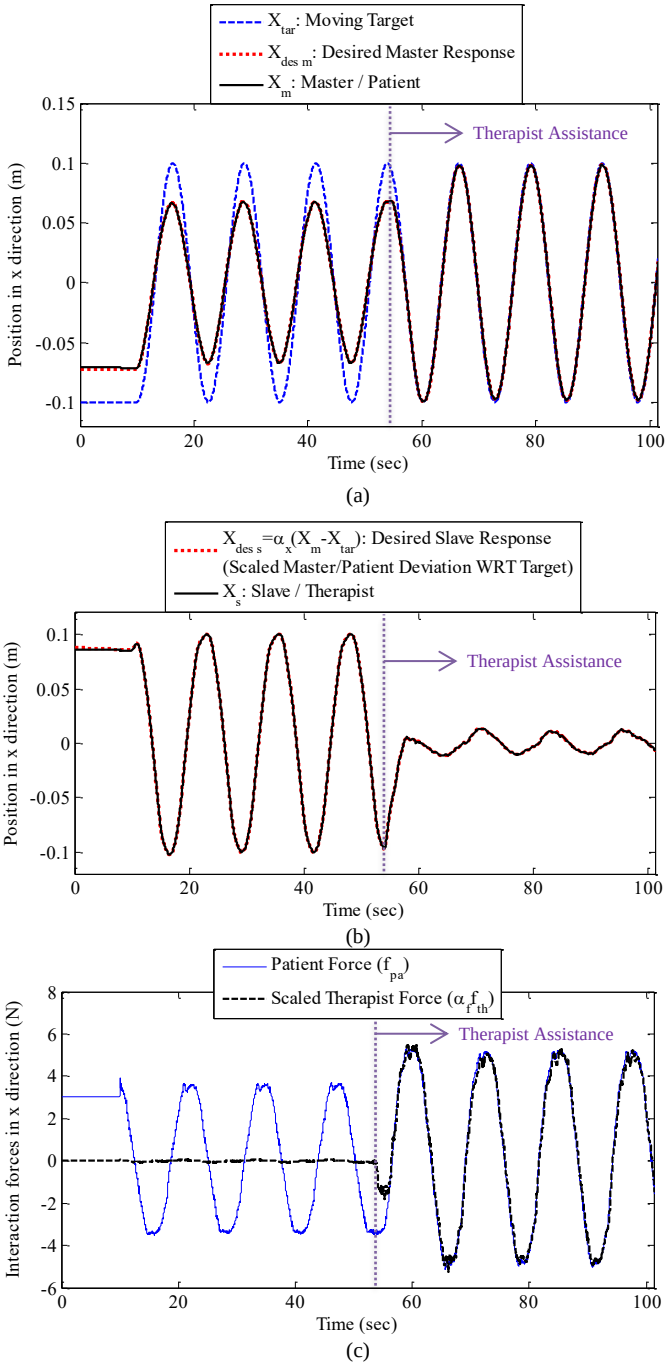


Fig. 12. (a) The desired and actual positions of the master robot ($\mathbf{x}_{des_m}$, $\mathbf{x}_m$), (b) the desired and actual positions of the slave robot ($\mathbf{x}_{des_s}$, $\mathbf{x}_s$), and (c) the patient's $\mathbf{f}_{pa}$ and the scaled therapist $\alpha_f \mathbf{f}_{th}$ forces (the assistive force of therapist has been applied from $t = 53.4$ sec), in $x$ direction for the Level 3 of assistance (introduced in Table 1).

### *6.1.2. Normal-Tangential to Cartesian Mapping*

Since the stiff environment as the virtual patient can apply a resistive force to the master robot toward the inside of the target's path (toward the origin as the equilibrium point of the springs set), the Normal-Tangential to Cartesian mapping can better interpret the centripetal patient's deviation for the therapist. As discussed in Sec. 2.5.2, the Normal-Tangential coordinates that rotate with the target in the desired path can express the patient's position deviation toward inside or outside the target's path, and/or forward or backward from the target in its path. Accordingly, the scaled patient-target deviation in the Normal-Tangential coordinates was mapped to the Cartesian space and then provided physically for the therapist using the slave robot and visually via the therapist's monitor (Fig. 13a). Similar to the previous Cartesian-Cartesian mapping shown in Fig. 6, the therapist was also informed visually in Fig. 13 about the position of the target in its desired path and visualize the patient's deviation corresponds to the Cartesian position.

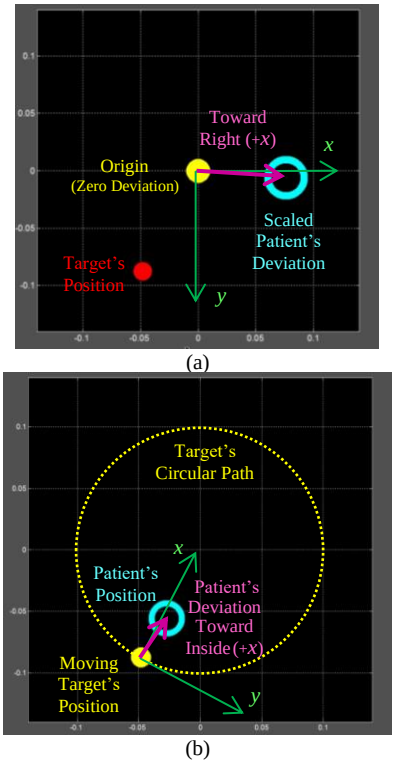


Fig. 13. Position data provided visually via (a) the therapist's and (b) the patient's monitors for the Normal-Tangential to Cartesian mapping during tracking the moving target using the proposed assist-as-needed tele-rehabilitation strategy (some notes are added).

The results of the proposed strategy with Normal-Tangential to Cartesian mapping (described in Sec. 2.6.2) are presented here for Level 2 of assistance (in Table 1). For this case, the master robot's position $\mathbf{x}_m$ in tracking its desired trajectory $\mathbf{x}_{des_m}$, and the target's position $\mathbf{x}_{tar}$ in $x$ direction of the Normal-Tangential space are shown in Fig. 14a. As illustrated in Figs. 13 and 3b, the $x$ direction in the Normal-Tangential coordinates for the master/patient is toward the inside of the target's path, and it is toward the right in the Cartesian coordinates for the slave/therapist. The slave robot's position $\mathbf{x}_s$ in tracking its desired trajectory $\mathbf{x}_{des_s}$ in $x$ direction of the Cartesian space is demonstrated in Fig. 14b. As seen in Fig. 14a and 14b, the therapist could successfully decrease the deviation of the virtual patient (stiff environment) from the target's position to zero $(\mathbf{x}_m - \mathbf{x}_{tar}) \to 0$ by adjusting his force $\mathbf{f}_{th}$ (Fig. 14c) after $t = 51.6$ sec. Using the suggested mapping between the Normal-Tangential and Cartesian coordinates, the therapist could guide the patient on the target's trajectory with higher accuracy (less value of $(\mathbf{x}_m - \mathbf{x}_{tar})$) in comparison with the Cartesian to Cartesian mapping (Figs. 7, 8, 11 and 12). The suitable performance of the therapist in convergence of the patient's position to the target ($\mathbf{x}_m \to \mathbf{x}_{tar}$) comes from interpretation of the patient-target deviation toward the inside (center) in the Normal-Tangential space to the right side in the Cartesian coordinates under the therapist's hand (see Fig. 13). The therapist could better adjust his assistive force $\mathbf{f}_{th}$ in this case (Fig. 14c) such that he neutralized the patient's force $\mathbf{f}_{th}$ more accurately in comparison with the previous case (Figs. 9, 11c and 12c). Consequently, the better force compensation $(\mathbf{f}_{pa} - \alpha_f \mathbf{f}_{th}) \to 0$ provided by the therapist (after $t = 51.6$ sec) resulted in the better target tracking by the patient $(\mathbf{x}_m - \mathbf{x}_{tar}) \to 0$ based on Eq. (2). The master and slave tracking errors are also demonstrated in Fig. 14d for this case of mapping.

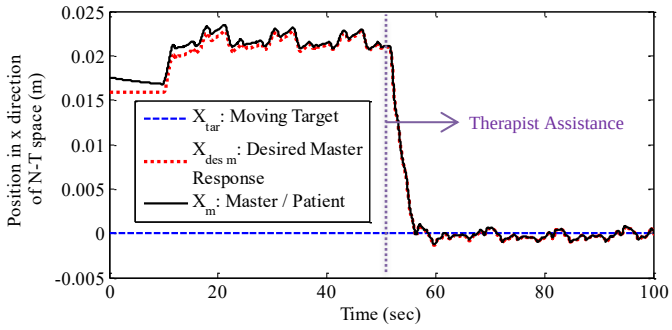


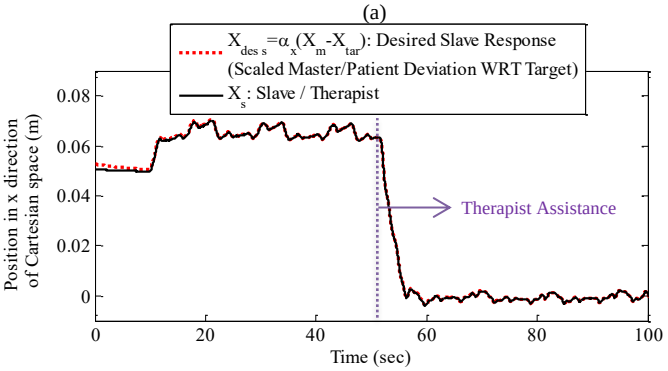


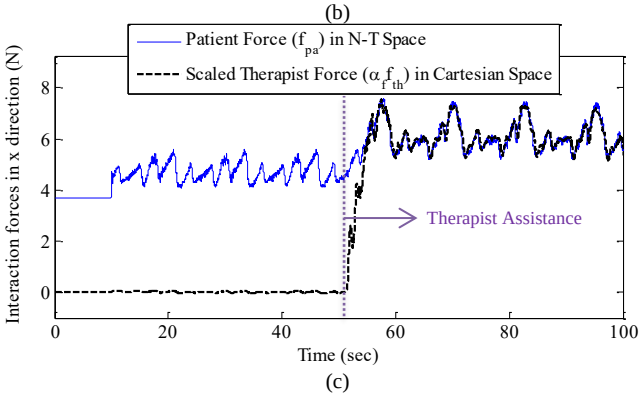


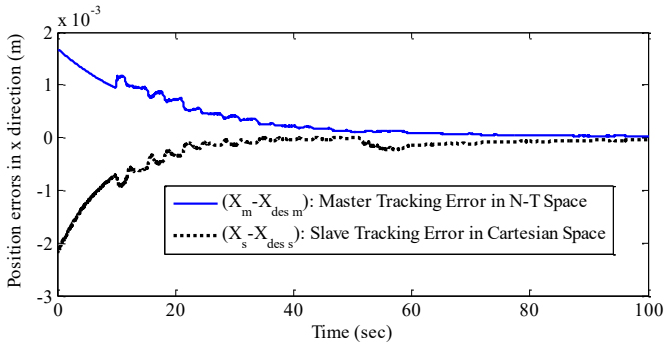


Fig. 14. (a) The desired and actual positions of the master robot/patient ( $\mathbf{x}_{des_m}$ , $\mathbf{x}_m$ ) in $x$ direction of the Normal-Tangential space, (b) the desired and actual positions of the slave robot/therapist ( $\mathbf{x}_{des_s}$ , $\mathbf{x}_s$ ) in $x$ direction of the Cartesian coordinates, (c) the patient's force $\mathbf{f}_{pa}$ and the scaled therapist force $\alpha_f \mathbf{f}_{th}$ (started from $t = 51.6$ sec ) in the Normal-tangential and Cartesian spaces, respectively, and (d) the master ( $\tilde{\mathbf{x}}_m = \mathbf{x}_m - \mathbf{x}_{des_m}$ ) and slave ( $\tilde{\mathbf{x}}_s = \mathbf{x}_s - \mathbf{x}_{des_s}$ ) tracking errors in the Normal-tangential and Cartesian spaces, respectively.

## 6.2. User Study (A Human Operator as the Patient)

In this section, the proposed robotic assist-as-needed tele-rehabilitation strategy is evaluated using an able-bodied human operator behaving as the patient, as shown in Fig. 15. In the following experiments, the performance of the proposed strategy with and without tremor filtration is investigated. These evaluations are presented for two levels of assistance and using different force/motion mappings.

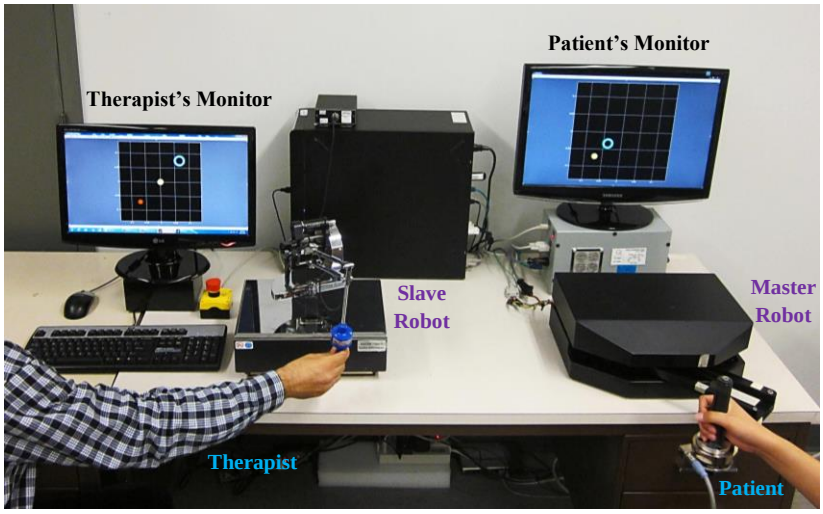


Fig. 15. The telerobotic experimental set-up for the second evaluations of assistive tele-rehabilitation strategy: the Quanser Rehab robot (right) is the master, the Phantom Premium robot (left) is the slave, and the patient is an able-bodied human operator.

### *6.2.1. Patient's Tremor Filtration*

In this part of the experiments, the natural frequency $\omega_n$ of desired impedance model (2), which is equal to the cut-off frequency (when $\zeta = 0.7$), was adjusted to be several times smaller than the minimum tremor frequency ($\omega_{trem_{\min}}$) as discussed in Sec. 2.4.1 such that the hand tremors of the patient were filtered out. The tremor simulated by the human operator (behaving as the patient) was tried to be in the range of realistic tremors of individuals having Parkinson's disease (PD), cerebral palsy (CP), multiple sclerosis (MS) and/or stroke. This frequency range of the rhythmic involuntary tremors is reported to be $\omega_{trem} \simeq 3-6$ Hz $= 18.85 - 37.70$ rad/sec in [49, 50]. For this purpose, the natural frequency of the impedance model (2) was adjusted such that $\omega_n \ll \omega_{trem_{\min}} = 18.85$ rad/sec. Therefore, the natural frequency of the desired impedance model (2) was chosen as $\omega_n = \sqrt{k_{des}/m_{des}} = 2$ rad/sec, which is about 10 times less than $\omega_{trem_{\min}} = 18.85$ rad/sec. Moreover, two different values of the stiffness parameter $k_{des}$ were chosen in this part of the experiments (see Table 3) to provide two levels of assistance for the patient in addition to the therapist's assistive force. Accordingly, using each value of $k_{des}$ and the adjusted $\omega_n = \sqrt{k_{des}/m_{des}} = 2$ rad/sec (for tremor filtration), and also $\zeta = c_{des}/2\sqrt{m_{des}k_{des}} = 0.7$ (for minimum overshoot), the values of damping $c_{des}$ and mass $m_{des}$ parameters were determined for each case, as presented in Table 3. The parameters of the proposed nonlinear bilateral control laws (9) and (10) and two adaptation laws (20) and (22) used in this part is the same as Sec. 6.1, presented in Table 2.

For Level 1 of assistance (Table 3) with tremor filtration, the desired and actual positions of the master robot/patient's hand ($\mathbf{x}_{des_m}$, $\mathbf{x}_m$) and the desired and actual position of the slave robot/therapist's hand ($\mathbf{x}_{des_s}$, $\mathbf{x}_s$) in the $y$ direction of the Cartesian space are shown in Fig. 16a and 16b, respectively. The master and slave tracking errors with respect to their corresponding desired trajectories are shown in Fig. 16c. Although the patient applied a considerable tremor-related high-frequency force to the master end-effector (demonstrated in Fig. 17), the high-frequency tremors of the patient are not seen in his position deviation with respect to the target (shown in Fig. 16b). This is due to the tremor filtration of the proposed strategy using the adjustment of the desired impedance model (2). As seen in Fig. 17, the scaled therapist's force $\alpha_f \mathbf{f}_{th}$ starting from $t = 53$ sec overcomes the low-frequency non-tremor portion of the patient's force $\mathbf{f}_{pa}$. In other words, the low-frequency portion of the patient's force is perceived by the therapist in this setting when he wants to bring the patient's position on the moving target's trajectory.

Table 3. The employed impedance parameters and scaling factors with and without patient's tremor filtration for two levels of assistance

| Level of Assistance | Desired Impedance Model Parameters | Scaling Factors |
|---|---|---|
| Level 1 (medium assistance) | $k_{des} = 200$ N/m<br>$c_{des} = 140$ N.s/m<br>$m_{des} = 50$ kg | $\alpha_f = 4$<br>$\alpha_x = 3$ |
| Level 2 (low assistance) | $k_{des} = 100$ N/m<br>$c_{des} = 70$ N.s/m<br>$m_{des} = 25$ kg | $\alpha_f = 4$<br>$\alpha_x = 3$ |

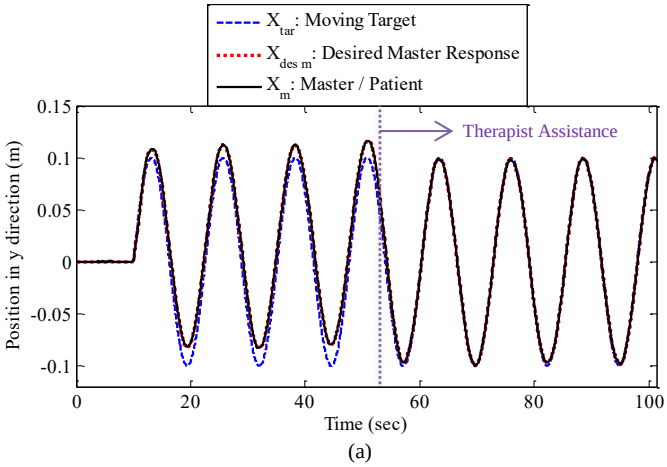

(a)

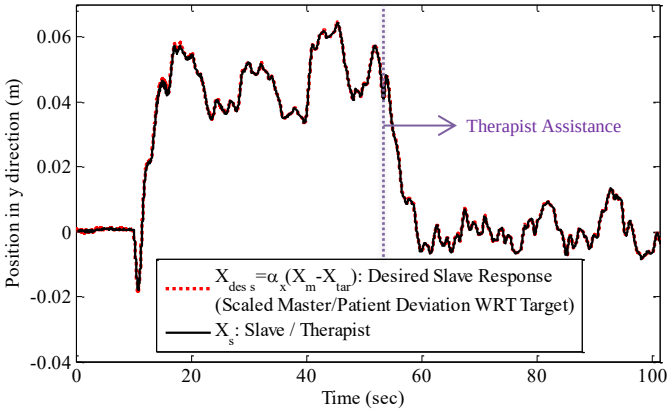


(b)

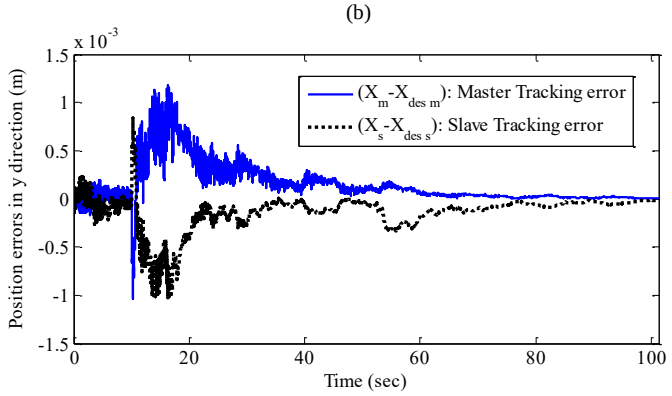


(c)

Fig. 16. (a) The desired and actual positions of the master robot/patient's hand ($\mathbf{x}_{des_m}$, $\mathbf{x}_m$), (b) the desired and actual positions of the slave robot/therapist's hand ($\mathbf{x}_{des_s}$, $\mathbf{x}_s$), and (c) the master ($\tilde{\mathbf{x}}_m = \mathbf{x}_m - \mathbf{x}_{des_m}$) and slave ($\tilde{\mathbf{x}}_s = \mathbf{x}_s - \mathbf{x}_{des_s}$) tracking errors, all in $y$ direction, for the Level 1 of assistance (introduced in Table 3) with filtration of the patient's tremor.

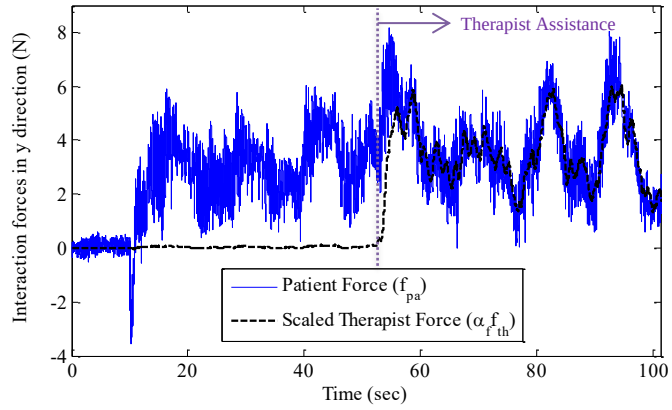


Fig. 17. The patient's force $\mathbf{f}_{pa}$ and the scaled therapist $\alpha_f \mathbf{f}_{th}$ force (starting from $t = 53$ sec) in $y$ direction, where the tremor-related high-frequency portion of the patient's force is not reflected to the therapist (tremor filtration).

Note that the performance of tremor filtration is the main difference between the experiments on a stiff environment (Sec. 6.1) and experiments with a human operator simulating patient tremors (Sec. 6.2). This difference is observed by comparing the results in Fig. 14 with the ones in Figs. 16 and 17. In other words, the high-frequency tremor-related part of the patient force (seen in Fig. 17) is appropriately filtered and do not affect the position trajectories (Fig. 16) significantly.

The desired ($\mathbf{x}_{des_m}$) and actual ($\mathbf{x}_m$) patient/master trajectories in the $x-y$ plane with respect to the circular trajectory ($\mathbf{x}_{tar}$) of the moving target are shown in Fig. 18a. In this figure, the deviated part of trajectories from the target corresponds to $t < 53$ sec, where the patient only had the assistance provided via the impedance elements ($k_{des}$, $c_{des}$ and $m_{des}$) based on Eq. (2). However, the part of trajectories in Fig. 18a, which is close to the target's trajectory, corresponds to $t > 53$ sec that the therapist adjusted his force (Fig. 17) to reduce the patient-deviation (see Fig. 16a and 16b). Also, the increase of the deviation with respect to target's trajectory by the patient and the decrease of this deviation by the therapist (at $t \approx 53$ sec) in the $x-y$ plane can be seen in Fig. 18b. Figure 18b shows the desired slave trajectory ($\mathbf{x}_{des_s}$ that is the scaled patient-target deviation) and the actual slave trajectory ($\mathbf{x}_s$) under the therapist's hand.

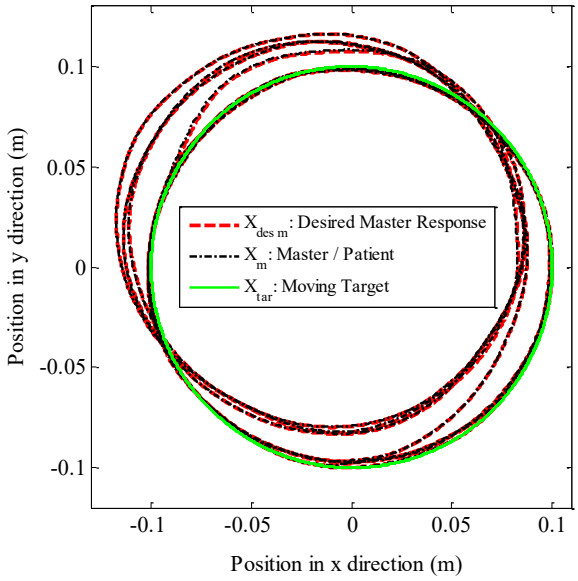


(a)

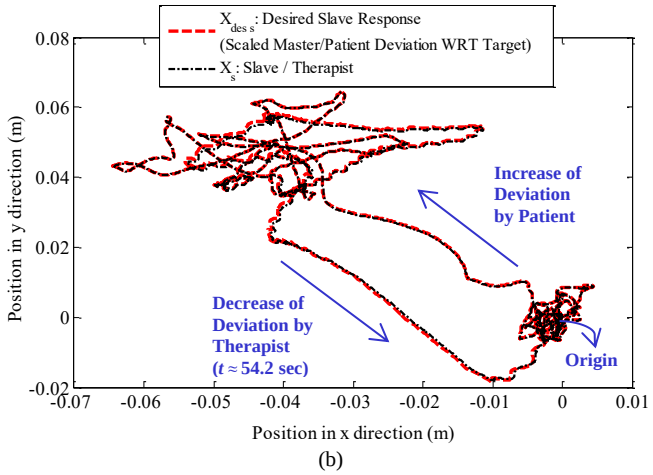


(b)

Fig. 18. (a) Desired ( $\mathbf{x}_{des_m}$ ) and actual ( $\mathbf{x}_m$ ) trajectories of the patient's hand (master end-effector) with respect to the circular trajectory ( $\mathbf{x}_{tar}$ ) of the moving target, and (b) desired ( $\mathbf{x}_{des_s}$ ) and actual ( $\mathbf{x}_s$ ) trajectories of the therapist's hand (slave end-effector), in the $x-y$ plane.

It should be noted that the amplitude of the therapist/slave motion or scaled patient deviation from the target trajectory in Fig. 16b or Fig. 18b is about 0.05 m (in each of $x$ and $y$ directions) before applying the therapist assistive force ( $t < 53$ sec ). However, it is decreased to 0.01 m after starting the therapist assistance ( $t > 53$ sec ) which is 10% of the amplitude of total patient/master motion trajectory in each of $x$ and $y$ directions (0.1 m in Fig. 16a or Fig. 18a). This feature can reduce the therapist's movements and consequently his fatigue in comparison with previous bilateral controllers [20, 21, 24, 32, 33] that made the same trajectory for the master and slave robots (patient and therapist), as discussed in Sec. 1, Sec. 2.3 and Sec. 2.5.

To elaborate more on this feature, the rate of spent mechanical energy by the therapist can be estimated in terms of his input power to the robot, which is formulated as the multiplication of the therapist force and the slave end-effector velocity. As seen in Figs. 8, 9, 11, 12, 14, 16-18, the slave/therapist motion range and velocity are minimized around origin/zero from the moment he started to apply the force. Therefore, the power consumption by the therapist is tried to be optimized using and the proposed strategy. This is due to tracking the master/patient deviation by the slave robot under the therapist's hand and decreasing this deviation to zero by his assistive force.

It is important the patient-target deviation $\mathbf{x}_m - \mathbf{x}_{tar}$ is originally small in comparison with the total patient $\mathbf{x}_m$ or moving target $\mathbf{x}_{tar}$ trajectories (Figs. 16a and 18a) based on the impedance model adjustments (discussed in Sec. 2.2, 2.4 and 2.5, and parameterized in Table 3 for the experiments). But this deviation is scaled up by the factor $\alpha_x$ (as discussed in Sec. 2.3), and the slave robot under the therapist's hand tracks the scaled (amplified) patient-target deviation $\mathbf{x}_s \rightarrow \alpha_x(\mathbf{x}_m - \mathbf{x}_{tar})$ to better reflect the patient's noncompliant motions to the therapist. Accordingly, the amplitude of the patient-target deviation in each of $x$ and $y$ directions is decreased to less than 0.0033 m in Figs. 16a and 18a after the therapist assistance ( $t > 53$ sec ), and using $\alpha_x = 3$ in Table 3. This deviation is scaled up and tracked by the therapist/slave, which has the amplitude of 0.01 m in Figs. 16b and 18b (after $t \approx 53$ sec ).

The patient/master and the therapist/slave positions for Level 2 of assistance (parameterized in Table 3) and with filtration of the patient's tremor are shown in Fig. 19a and 19b, respectively. The performance of the high-frequency force filtration from the haptic force feedback provided for the therapist is observed in Fig. 19c. Since the impedance parameters decreased 50% from Level 1 to Level 2, as mentioned in Table 3, the patient's flexibility in Level 2 is two times the one in Level 1 (before the intervention of the therapist via applying the force $\mathbf{f}_{th}$ ). In other words, the magnitude of the patient's deviation from the target in response to a specified value of the applied patient's force ( $\mathbf{f}_{pa}$ in Figs. 17 and 19c) is two times larger in the Level 2 (Fig. 19b) in comparison with the Level 1 (Fig. 16b). As a result, the assistive force provided for the patient by the impedance elements decreased by 50% from Level 1 to 2 (before applying the therapist's assistive force). This decrease of the patient's assistance can be performed in future patient rehabilitation considering his motor recovery and improvements during the process.

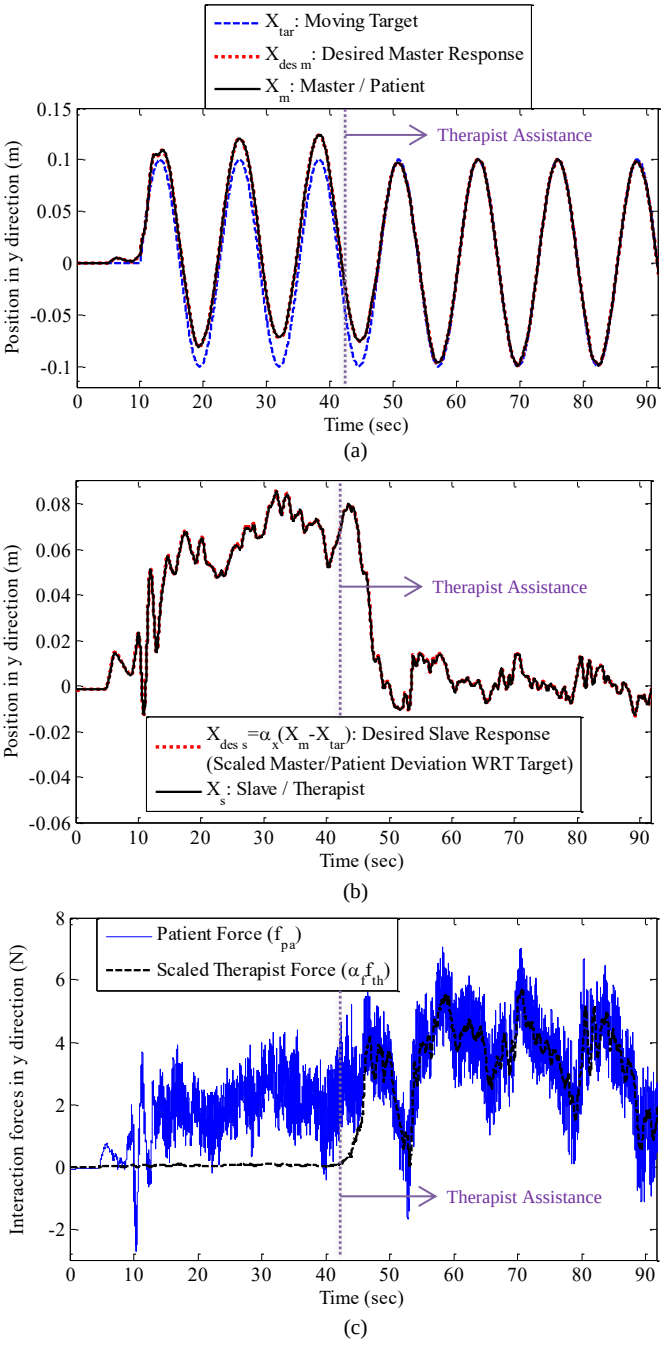


Fig. 19. (a) Desired and actual positions of the master robot ( $\mathbf{x}_{des_m}$ , $\mathbf{x}_m$ ) , (b) desired and actual positions of the slave robot ( $\mathbf{x}_{des_s}$ , $\mathbf{x}_s$ ), and (c) the patient's $\mathbf{f}_{pa}$ and the scaled therapist $\alpha_f \mathbf{f}_{th}$ forces with tremor filtration, in $y$ direction for the Level 2 of assistance (parameterized in Table 3).

### *6.2.2. Patient's Tremor Reflection*

Finally, the performance of the proposed robotic tele-rehabilitation strategy is evaluated when the patient's tremor is not filtered from the patient's hand trajectory (by the master robot) and it is instead desired to be reflected to the therapist' hand (via the slave robot). In this case, the tremor-related high-frequency portion of the patient's force $\mathbf{f}_{pa}$ should not be filtered via the impedance model (2). In other words, the natural frequency of the desired impedance model (2) should be adjusted such that $\omega_n \geq \omega_{trem}$ (as discussed in Sec. 2.4.2). Considering the range of patient's tremor frequency as $\omega_{trem} \simeq 3-6 \text{ Hz} = 18.85-37.70 \text{ rad/sec}$ [49, 50], the natural frequency of the impedance model (2) was chosen $\omega_n = 40 \text{ rad/sec}$ to be larger than $\omega_{trem}$. Moreover, using the stiffness parameter $k_{des}$ =100 N/m similar to Level 2 (in Table 3), and employing $\omega_n = \sqrt{k_{des}/m_{des}} = 40 \text{ rad/sec}$ (for tremor reflection) and $\zeta = c_{des}/2\sqrt{m_{des}k_{des}} = 0.7$ (for minimum overshoot), the damping and mass parameters were obtained as $c_{des}$ =3.5 N.s/m and $m_{des}$ =0.0625 kg , respectively. The position and force scaling factors were the same as ones in the previous section ( $\alpha_x = 3$ and $\alpha_f = 4$ ). However, the Normal-Tangential to Cartesian mapping (presented in Sec. 2.5.2) was employed in this experiment.

Using the above-mentioned impedance adjustment, the patient's tremor affected his position deviations from the target's trajectory, as shown in Fig. 20a. As a result, these tremors (high-frequency movements) were reflected (transmitted) to the therapist's hand via the slave robot as seen in Fig. 20b. After $t \approx 47.2$ sec when the therapist tried to decrease the patient's deviation (Fig. 20a and 20b), the patient's tremor-related high-frequency force was also perceived by the therapist (Fig. 20c).

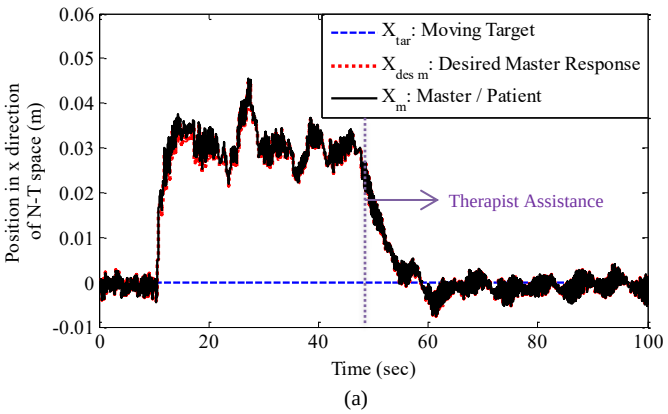

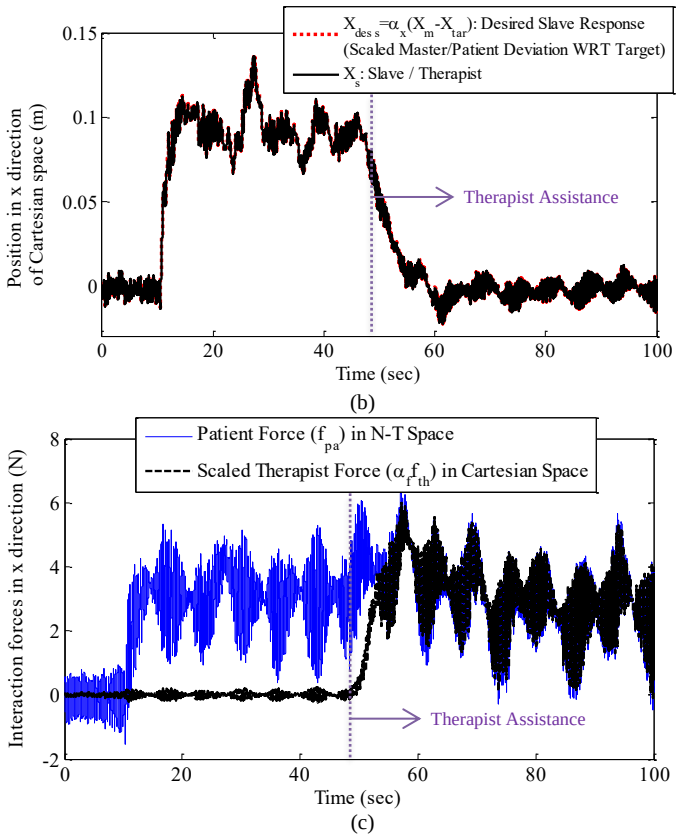


Fig. 20. (a) Desired and actual positions of the master/patient ( $\mathbf{x}_{des_m}$ , $\mathbf{x}_m$ ) , (b) desired and actual positions of the slave/therapist ( $\mathbf{x}_{des_s}$ , $\mathbf{x}_s$ ), and (c) the patient's $\mathbf{f}_{pa}$ and the scaled therapist $\alpha_f \mathbf{f}_{th}$ forces, in $x$ direction, without tremor filtration (with the reflection of high-frequency force).

Note that the high-frequency part of the patient-master force signals (in Fig. 17, Fig. 19c and Fig. 20c) is due to the simulated patient tremor (in the range of $3-6$ Hz [49, 50]), and the ATI Gamma sensor (as a precise force/torque sensor attached to the master robot) do not have such noises with a considerable amplitude (about 1 N).

The proposed bilateral control strategy is experimentally evaluated in this work for upper-limb tele-rehabilitation of a simulated patient. However, it can be utilized in robotic rehabilitation process of lower-limb cases with appropriate selection of the moving target trajectory $\mathbf{x}_{tar}$, without loss of generality.

## 7. Conclusion

In this paper, a new assist-as-needed tele-rehabilitation strategy was proposed by facilitating an impedance-based collaboration between a patient and a therapist using a multi-DOF master-slave telerobotic system. In this strategy, the combination of the patient's and therapist's forces specifies the patient's admissible deviation from a moving target trajectory based on an impedance model. Two adjustable sources of haptics-based assistance are provided to the patient for following the moving target's trajectory via the master robot: a) the designed impedance elements (including stiffness, damping and mass) that modulate the level of assist-as-needed behavior of the robotic system, and b) the online scaled force of the therapist applied to the slave robot, by which he/she can intervene online in the patient's movement therapy exercises through the haptic force feedback loop.

In this scheme, the therapist/slave only tracks the deviation of the patient/master from the target's trajectory and not the total patient's hand trajectory. This feature minimizes the therapist's movements and consequently, his/her fatigue while the patient follows the specified target trajectory as part of the rehabilitation program.

The proposed desired impedance model can be adjusted based on the patient's symptoms and disabilities. Accordingly, two cases of impedance adjustment for the patients suffering from insufficient actuation of muscles and involuntary tremors were presented. Moreover, two cases of force/motion mapping between the patient/master and the therapist/slave were introduced and tested. The first one was defined in the Cartesian space and the second one was presented between the Cartesian and Normal-Tangential coordinates. One of these choices can be selected by the therapist due to his convenience and/or the patient's characteristics.

A nonlinear bilateral robust adaptive controller was designed such that the multi-DOF master and slave robots can track their corresponding desired trajectories. The master and slave tracking convergence together with the stability and robustness of the controlled nonlinear teleoperation system in the presence of parametric (structured) and non-parametric (unstructured)

uncertainties are guaranteed theoretically using the Lyapunov stability method and verified experimentally. Based on the stability of the desired impedance model and the Lyapunov stability of the closed-loop nonlinear dynamics of the telerobotic system, the safety of the patient and therapist during the tele-rehabilitation is enhanced.

Comprehensive experimental evaluations were performed using the Quanser Rehab robot as the master and the Phantom Premium robot as the slave. In these experiments, either a stiff environment (made by a set of springs) or an actual human operator behaves as the patient in different evaluations. Different adjustments of the impedance model and force/motion mapping introduced for the proposed assist-as-needed tele-rehabilitation strategy were tested. These adjustments provided different assistance levels for the patient and could filter or reflect the patient's tremor based on the therapist's decision.

Having these promising results from the proposed controller and its experimental evaluations with the involvement of healthy subjects, the assessment of the system will be performed in our future works in realistic clinical settings with the participation of patients having physical impairments. The proposed tele-rehabilitation strategy can also be evaluated in future studies considering the movements in activities of daily living (ADL) as the target point trajectory for the patient. This strategy can also be implemented in different rehabilitation tasks to collect the therapist's position, force and impedance adjustment behavior in assisting a group of patients. Then, autonomous therapeutic assistance can be programmed via Machine Learning (ML) methods based on the task-specific data of the human therapist obtained via the proposed tele-rehabilitation scheme. This artificial automatic therapist will further decrease the intervention of the human therapist and the requirement of the slave robot. In addition, it will be capable of predicting the patient's behavior and assisting him/her intelligently using fast computer processing in order to follow the task targets accurately.

There is not any packet loss and/or communication delay (higher than the adjusted sampling time) for signal transmission in the employed experimental teleoperation set-up. Accordingly, these inaccuracies are not considered in the controller design and the stability analysis, considering both the therapist and patient in the same clinical setting. However, this issue (existence of packet loss and/or time delay in communication channels) can be studied in future works on tele-rehabilitation systems that have a long distance between master and slave robots and/or have non-ideal communications for the signal transmission.

## Appendix. Master and Slave Dynamics and Control Laws in the Joint Space

The dynamics of the multi-DOF master and slave robots in the joint space is presented as [51]

$$\mathbf{M}_{\mathbf{q},m}(\mathbf{q}_m)\ddot{\mathbf{q}}_m + \mathbf{C}_{\mathbf{q},m}(\mathbf{q}_m,\dot{\mathbf{q}}_m)\dot{\mathbf{q}}_m + \mathbf{G}_{\mathbf{q},m}(\mathbf{q}_m) + \mathbf{F}_{\mathbf{q},m}(\dot{\mathbf{q}}_m) = \boldsymbol{\tau}_m + \boldsymbol{\tau}_{pa} + \mathbf{u}_{\mathbf{q},m} \tag{A1}$$

$$\mathbf{M}_{\mathbf{q},s}(\mathbf{q}_s)\ddot{\mathbf{q}}_s + \mathbf{C}_{\mathbf{q},s}(\mathbf{q}_s,\dot{\mathbf{q}}_s)\dot{\mathbf{q}}_s + \mathbf{G}_{\mathbf{q},s}(\mathbf{q}_s) + \mathbf{F}_{\mathbf{q},s}(\dot{\mathbf{q}}_s) = \boldsymbol{\tau}_s - \boldsymbol{\tau}_{th} + \mathbf{u}_{\mathbf{q},s} \tag{A2}$$

Using the subscript $i = m$ for the master and $i = s$ for the slave, the kinematic transformations between the joint space and the Cartesian space are expressed for each robot as

$$\mathbf{x}_i = \Omega_i(\mathbf{q}_i),\ \ \dot{\mathbf{x}}_i = \mathbf{J}_i(\mathbf{q}_i)\dot{\mathbf{q}}_i,\ \ \ddot{\mathbf{x}}_i = \mathbf{J}_i(\mathbf{q}_i)\ddot{\mathbf{q}}_i + \dot{\mathbf{J}}_i(\mathbf{q}_i)\dot{\mathbf{q}}_i \tag{A3}$$

where $\mathbf{J}_i(\mathbf{q}_i) = d\Omega_i(\mathbf{q}_i)\big/ d\,\mathbf{q}_i$ is the Jacobian matrix. The relations of the dynamic matrices and vectors between the joint space (Eqs. (A1) and (A2)) and the Cartesian space (Eqs. (3) and (4)) are presented as

$$\begin{aligned}
&\mathbf{M}_{\mathbf{x},i}(\mathbf{q}_i) = \mathbf{J}_i^{-T}\mathbf{M}_{\mathbf{q},i}(\mathbf{q}_i)\mathbf{J}_i^{-1},\quad \mathbf{G}_{\mathbf{x},i}(\mathbf{q}_i) = \mathbf{J}_i^{-T}\mathbf{G}_{\mathbf{q},i}(\mathbf{q}_i)\\
&\mathbf{C}_{\mathbf{x},i}(\mathbf{q}_i,\dot{\mathbf{q}}_i) = \mathbf{J}_i^{-T}\left(\mathbf{C}_{\mathbf{q},i}(\mathbf{q}_i,\dot{\mathbf{q}}_i) - \mathbf{M}_{\mathbf{q},i}(\mathbf{q}_i)\mathbf{J}_i^{-1}\dot{\mathbf{J}}_i\right)\mathbf{J}_i^{-1}\\
&\mathbf{F}_{\mathbf{x},i}(\mathbf{q}_i) = \mathbf{J}_i^{-T}\mathbf{F}_{\mathbf{q},i}(\mathbf{q}_i),\quad \mathbf{u}_{\mathbf{x},i} = \mathbf{J}_i^{-T}\mathbf{u}_{\mathbf{q},i}\\
&\mathbf{f}_i = \mathbf{J}_i^{-T}\boldsymbol{\tau}_i,\quad \mathbf{f}_{th} = \mathbf{J}_m^{-T}\boldsymbol{\tau}_{th},\quad \mathbf{f}_{pa} = \mathbf{J}_s^{-T}\boldsymbol{\tau}_{pa}
\end{aligned} \tag{A4}$$

Also, the representation of the control laws (9) and (10) in the joint space are obtained in terms of the joint space's matrices and vectors by substituting (A4) in (9) and (10) as

$$\begin{aligned}\boldsymbol{\tau}_m = &-\beta_{3,m}\,\hat{\mathbf{M}}_{\mathbf{q},m}(\mathbf{q}_m)\,\mathbf{J}_m^{-1}\boldsymbol{\varepsilon}_m \\ &+\hat{\mathbf{M}}_{\mathbf{q},m}(\mathbf{q}_m)\,\mathbf{J}_m^{-1}\left(\ddot{\mathbf{x}}_{ref,m}-\dot{\mathbf{J}}_m\,\mathbf{J}_m^{-1}\,\dot{\mathbf{x}}_{ref,m}\right) \\ &+\hat{\mathbf{C}}_{\mathbf{q},m}(\mathbf{q}_m,\dot{\mathbf{q}}_m)\,\mathbf{J}_m^{-1}\,\dot{\mathbf{x}}_{ref,m}+\hat{\mathbf{G}}_{\mathbf{q},m}(\mathbf{q}_m)+\hat{\mathbf{F}}_{\mathbf{q},m}(\dot{\mathbf{q}}_m) \\ &-\mathbf{J}_m^T\,\mathbf{f}_{pa}-\mathbf{J}_m^T\,\hat{\gamma}_m\,\mathrm{sgn}(\boldsymbol{\varepsilon}_m)\end{aligned} \tag{A5}$$

$$\begin{aligned}\boldsymbol{\tau}_s = &-\beta_{3,s}\,\hat{\mathbf{M}}_{\mathbf{q},s}(\mathbf{q}_s)\,\mathbf{J}_s^{-1}\boldsymbol{\varepsilon}_s \\ &+\hat{\mathbf{M}}_{\mathbf{q},s}(\mathbf{q}_s)\,\mathbf{J}_s^{-1}\left(\ddot{\mathbf{x}}_{ref,s}-\dot{\mathbf{J}}_s\,\mathbf{J}_s^{-1}\,\dot{\mathbf{x}}_{ref,s}\right) \\ &+\hat{\mathbf{C}}_{\mathbf{q},s}(\mathbf{q}_s,\dot{\mathbf{q}}_s)\,\mathbf{J}_s^{-1}\,\dot{\mathbf{x}}_{ref,s}+\hat{\mathbf{G}}_{\mathbf{q},s}(\mathbf{q}_s)+\hat{\mathbf{F}}_{\mathbf{q},s}(\dot{\mathbf{q}}_s) \\ &+\mathbf{J}_s^T\,\mathbf{f}_{th}-\mathbf{J}_s^T\,\hat{\gamma}_s\,\mathrm{sgn}(\boldsymbol{\varepsilon}_s)\end{aligned} \tag{A6}$$

These input torques (A5) and (A6) are applied by the motors in the joint space of master and slave robots.

## References


[1] World Health Organization (WHO), "The top 10 causes of death," ed. http://www.who.int/mediacentre/factsheets/fs310/en/, 2014.

[2] D. Mozaffarian, E. J. Benjamin, A. S. Go, D. K. Arnett, M. J. Blaha, M. Cushman, *et al.*, "Heart disease and stroke statistics—2015 update: A report from the American Heart Association," *Circulation*, vol. 131, pp. e29-e322, 2015.

[3] K. N. Arya, S. Pandian, R. Verma, and R. K. Garg, "Movement therapy induced neural reorganization and motor recovery in stroke: A review," *Journal of Bodywork and Movement Therapies*, vol. 15, pp. 528-537, 2011.

[4] P. M. Rossini, C. Calautti, F. Pauri, and J. C. Baron, "Post-stroke plastic reorganisation in the adult brain," *The Lancet Neurology*, vol. 2, pp. 493-502, 2003.

[5] A. A. Blank, J. A. French, A. U. Pehlivan, and M. K. O'Malley, "Current trends in robot-assisted upper-limb stroke rehabilitation: Promoting patient engagement in therapy," *Current Physical Medicine and Rehabilitation Reports*, vol. 2, pp. 184-195, 2014.

[6] H. I. Krebs and N. Hogan, "Robotic therapy: The tipping Point," *American journal of physical medicine & rehabilitation / Association of Academic Physiatrists*, vol. 91, pp. S290-S297, 2012.

[7] A. Gupta and M. K. O'Malley, "Design of a haptic arm exoskeleton for training and rehabilitation," *Mechatronics, IEEE/ASME Transactions on*, vol. 11, pp. 280-289, 2006.

[8] W. Meng, Q. Liu, Z. Zhou, Q. Ai, B. Sheng, and S. Xie, "Recent development of mechanisms and control strategies for robot-assisted lower limb rehabilitation," *Mechatronics*, vol. 31, pp. 132-145, 2015.

[9] S. E. Fasoli, H. I. Krebs, and N. Hogan, "Robotic technology and stroke rehabilitation: Translating research into practice," *Topics in Stroke Rehabilitation*, vol. 11, pp. 11-19, 2004.

[10] N. Hogan, H. I. Krebs, A. Sharon, and J. Charnnarong, "Interactive robotic therapist," ed: Google Patents, 1995.

[11] H. I. Krebs, B. T. Volpe, D. Williams, J. Celestino, S. K. Charles, D. Lynch, *et al.*, "Robot-aided neurorehabilitation: A robot for wrist rehabilitation," *Neural Systems and Rehabilitation Engineering, IEEE Transactions on*, vol. 15, pp. 327-335, 2007.

[12] R. Riener, T. Nef, and G. Colombo, "Robot-aided neurorehabilitation of the upper extremities," *Medical and Biological Engineering and Computing*, vol. 43, pp. 2-10, 2005.

[13] A. Gupta, M. K. O'Malley, V. Patoglu, and C. Burgar, "Design, control and performance of RiceWrist: A force feedback wrist exoskeleton for rehabilitation and training," *The International Journal of Robotics Research*, vol. 27, pp. 233-251, 2008.

[14] C. R. Carignan and H. I. Krebs, "Telerehabilitation robotics: Bright lights, big future?," *Journal of Rehabilitation Research and Development*, vol. 43, pp. 695-710, 2006.

[15] M. Johnson, R. V. Loureiro, and W. Harwin, "Collaborative tele-rehabilitation and robot-mediated therapy for stroke rehabilitation at home or clinic," *Intelligent Service Robotics*, vol. 1, pp. 109-121, 2008.

[16] V. G. Popescu, G. C. Burdea, M. Bouzit, and V. R. Hentz, "A virtual-reality-based telerehabilitation system with force feedback," *Information Technology in Biomedicine, IEEE Transactions on*, vol. 4, pp. 45-51, 2000.

[17] D. J. Reinkensmeyer, C. T. Pang, J. A. Nessler, and C. C. Painter, "Web-based telerehabilitation for the upper extremity after stroke," *Neural Systems and Rehabilitation Engineering, IEEE Transactions on*, vol. 10, pp. 102-108, 2002.

[18] C. Jadhav and V. Krovi, "A low-cost framework for individualized interactive telerehabilitation," in *Engineering in Medicine and Biology Society. IEMBS. 26th Annual International Conference of the IEEE*, pp. 3297-3300, 2004.

[19] J. Kim, H. Kim, B. K. Tay, M. Muniyandi, M. A. Srinivasan, J. Jordan, *et al.*, "Transatlantic touch: A study of haptic collaboration over long distance," *Presence: Teleoperators and Virtual Environments*, vol. 13, pp. 328-337, 2004.

[20] C. Basdogan, C. H. Ho, M. A. Srinivasan, and M. Slater, "An experimental study on the role of touch in shared virtual environments," *ACM Trans. Comput.-Hum. Interact.*, vol. 7, pp. 443-460, 2000.

[21] R. Tao, "Haptic teleoperation based rehabilitation systems for task-oriented therapy," M.Sc. Thesis, Department of Electrical and Computer Engineering, University of Alberta, 2014.

[22] M. Shahbazi, S. F. Atashzar, M. Tavakoli, and R. V. Patel, "Therapist-in-the-loop robotics-assisted mirror rehabilitation therapy: An Assist-as-Needed framework," in *Robotics and Automation (ICRA), IEEE International Conference on*, pp. 5910-5915, 2015.

[23] S. F. Atashzar, M. Shahbazi, M. Tavakoli, and R. V. Patel, "A new passivity-based control technique for safe patient-robot interaction in haptics-enabled rehabilitation systems," in *Intelligent Robots and Systems (IROS), IEEE/RSJ International Conference on*, pp. 4556-4561, 2015.

[24] C. R. Carignan and P. A. Olsson, "Cooperative control of virtual objects over the Internet using force-reflecting master arms," in *Robotics and Automation. ICRA. IEEE International Conference on*, pp. 1221-1226, 2004.

[25] J. E. Colgate, "Robust impedance shaping telemanipulation," *Robotics and Automation, IEEE Transactions on*, vol. 9, pp. 374-384, 1993.

[26] L. Dongjun and P. Y. Li, "Passive bilateral feedforward control of linear dynamically similar teleoperated manipulators," *Robotics and Automation, IEEE Transactions on*, vol. 19, pp. 443-456, 2003.

[27] D. A. Lawrence, "Stability and transparency in bilateral teleoperation," *Robotics and Automation, IEEE Transactions on*, vol. 9, pp. 624-637, 1993.

[28] I. G. Polushin, P. X. Liu, C.-H. Lung, and G. D. On, "Position-error based schemes for bilateral teleoperation with time delay: Theory and experiments," *Journal of Dynamic Systems, Measurement, and Control*, vol. 132, p. 031008 (11 pages), 2010.

[29] N. Chopra, M. W. Spong, and R. Lozano, "Synchronization of bilateral teleoperators with time delay," *Automatica*, vol. 44, pp. 2142-2148, 2008.

[30] E. Nuño, R. Ortega, and L. Basañez, "An adaptive controller for nonlinear teleoperators," *Automatica*, vol. 46, pp. 155-159, 2010.

[31] Y. C. Liu and N. Chopra, "Control of semi-autonomous teleoperation system with time delays," *Automatica*, vol. 49, pp. 1553-1565, 2013.

[32] J. H. Ryu and D. S. Kwon, "A novel adaptive bilateral control scheme using similar closed-loop dynamic characteristics of master/slave manipulators," *Journal of Robotic Systems*, vol. 18, pp. 533-543, 2001.

[33] X. Liu and M. Tavakoli, "Adaptive inverse dynamics four-channel control of uncertain nonlinear teleoperation systems," *Advanced Robotics*, vol. 25, pp. 1729-1750, 2011.

[34] N. Hogan, "Impedance control: An approach to manipulation: Part I---Theory," *Journal of Dynamic Systems, Measurement, and Control*, vol. 107, pp. 1-7, 1985.

[35] A. Abdossalami and S. Sirouspour, "Adaptive control for improved transparency in haptic simulations," *Haptics, IEEE Transactions on*, vol. 2, pp. 2-14, 2009.

[36] M. Sharifi, S. Behzadipour, and G. R. Vossoughi, "Model reference adaptive impedance control of rehabilitation robots in operational space," in *Biomedical Robotics and Biomechatronics (BioRob), 4th IEEE RAS & EMBS International Conference on*, pp. 1698-1703, 2012.

[37] H. I. Krebs, J. J. Palazzolo, L. Dipietro, M. Ferraro, J. Krol, K. Rannekleiv, *et al.*, "Rehabilitation robotics: Performance-based progressive robot-assisted therapy," *Autonomous Robots*, vol. 15, pp. 7-20, 2003.
[38] A. Rubio, A. Avello, and J. Florez, "Adaptive impedance modification of a master-slave manipulator," in *Robotics and Automation. Proceedings. IEEE International Conference on*, pp. 1794-1799, 1999.
[39] R. V. Dubey, C. Tan Fung, and S. E. Everett, "Variable damping impedance control of a bilateral telerobotic system," *Control Systems, IEEE*, vol. 17, pp. 37-45, 1997.
[40] K. Hashtrudi-Zaad and S. E. Salcudean, "Analysis of control architectures for teleoperation systems with impedance/admittance master and slave manipulators," *The International Journal of Robotics Research*, vol. 20, pp. 419-445, 2001.
[41] H. C. Cho and J. H. Park, "Stable bilateral teleoperation under a time delay using a robust impedance control," *Mechatronics*, vol. 15, pp. 611-625, 2005.
[42] J. J. Abbott and A. M. Okamura, "Pseudo-admittance bilateral telemanipulation with guidance virtual fixtures," *The International Journal of Robotics Research*, vol. 26, pp. 865-884, 2007.
[43] X. Liu and M. Tavakoli, "Adaptive control of teleoperation systems with linearly and nonlinearly parameterized dynamic uncertainties," *Journal of Dynamic Systems, Measurement, and Control*, vol. 134, p. 021015 (10 pages), 2012.
[44] F. Hashemzadeh, M. Sharifi, and M. Tavakoli, "Nonlinear trilateral teleoperation stability analysis subjected to time-varying delays," *Control Engineering Practice*, vol. 56, pp. 123-135, 2016.
[45] M. Shahbazi, S. F. Atashzar, and R. V. Patel, "A framework for supervised robotics-assisted mirror rehabilitation therapy," in *IEEE/RSJ International Conference on Intelligent Robots and Systems (IROS)*, pp. 3567-3572, 2014.
[46] M. Sharifi, S. Behzadipour, H. Salarieh, and M. Tavakoli, "Cooperative modalities in robotic tele-rehabilitation using nonlinear bilateral impedance control," *Control Engineering Practice*, vol. 67, pp. 52-63, 2017.
[47] M. Shahbazi, S. F. Atashzar, M. Tavakoli, and R. V. Patel, "Robotics-assisted mirror rehabilitation therapy: A therapist-in-the-loop assist-as-needed architecture," *IEEE/ASME Transactions on Mechatronics*, vol. 21, pp. 1954-1965, 2016.
[48] M. Sharifi, H. Salarieh, S. Behzadipour, and M. Tavakoli, "Patient-robot-therapist collaboration using resistive impedance controlled tele-robotic systems subjected to time delays," *Journal of Mechanisms and Robotics*, vol. 10, pp. 061003 (17 pages), 2018.
[49] S. Bansil, N. Prakash, J. Kaye, S. Wrigley, C. Manata, C. Stevens-haas, *et al.*, "Movement Disorders after Stroke in Adults: A Review," *Tremor and other hyperkinetic movements*, vol. 2, pp. tre-02-42-195-1, 2012.
[50] S. Smaga, "Tremor," *American Family Physician*, vol. 68, pp. 1545-1552, 2003.
[51] J. J. E. Slotine and W. Li, *Applied nonlinear control*. NJ, Englewood Cliffs: Prantice-Hall, 1991.
[52] X. Liu, R. Tao, and M. Tavakoli, "Adaptive control of uncertain nonlinear teleoperation systems," *Mechatronics*, vol. 24, pp. 66-78, 2014.
[53] M. Sharifi, S. Behzadipour, and G. R. Vossoughi, "Model reference adaptive impedance control in Cartesian coordinates for physical human–robot interaction," *Advanced Robotics*, vol. 28, pp. 1277-1290, 2014.
[54] M. D. Dyck, "Measuring the dynamic impedance of the human arm," M.Sc. Thesis, Department of Electrical and Computer Engineering, University of Alberta, 2013.
[55] M. Dyck and M. Tavakoli, "Measuring the dynamic impedance of the human arm without a force sensor," in *Rehabilitation Robotics (ICORR), IEEE International Conference on*, pp. 1-8, 2013.
[56] M. C. Çavuşoğlu, D. Feygin, and F. Tendick, "A critical study of the mechanical and electrical properties of the PHANToM haptic interface and improvements for high-performance control," *Presence: Teleoperators & Virtual Environments*, vol. 11, pp. 555-568, 2002.